**SUPPLEMENTAL TABLE 6.** Electrophysiologic Group Transition and ABCA4 Variantsa Identified in 59 Patients With Stargardt Disease (*Continued*)

| Pt | Electrophysiologic Group (BL / FU) | Genotype Group | Number of Variants | Exon | Nucleotide Substitution | Amino Acid Change | Screening Method (Yes/No) | | |
|---|---|---|---|---|---|---|---|---|---|
| | | | | | | | SSCP | APEX | DS |
| 35 | II / II | B | 2 | 3 | c.161 G>A | p.Cys54Tyr | ✓ | — | — |
| | | | | 17 | c.2588 G>C | p.Gly863Ala | ✓ | — | — |
| 36 | II / II | A | 2 | 19 | c.2791 G>A | p.Val931Met | — | ✓ | — |
| | | | | Int. 38 | c.5461-10 T>C | Splice site | — | ✓ | — |
| 37 | II / III | C | 1 | 28 | c.4139 C>T | p.Pro1380Leu | — | ✓ | — |
| 38 | II / III | A | 2 | 22 | c.3211_3212insGT | p.Ser1071Cysfs*1084 | — | ✓ | — |
| | | | | 28 | c.4139 C>T | p. Pro1380Leu | — | ✓ | — |
| 39 | II / III | A | 2 | Int. 38 | c.5461-10 T>C | Splice site | — | ✓ | — |
| | | | | Int. 40 | c.5714+5 G>A | Splice site | — | ✓ | — |
| 40 | II / III | D | 0 | | | | ✓ | — | — |
| 41 | II / III | D | 0 | | | | ✓ | — | — |
| 42 | II / III | C | 1 | 3 | c.161 G>A | p.Cys54Tyr | ✓ | — | — |
| 43 | II / III | D | 0 | | | | ✓ | — | — |
| 44 | II / III | C | 1 | 19 | c.2894 A>G | p.Asn965Ser | ✓ | — | — |
| 45 | III / III | C | 1 | 21 | c.3056 C>T | p.Thr1019Met | ✓ | — | — |
| 46 | III / III | C | 1 | 21 | c.3056 C>T | p.Thr1019Met | ✓ | — | — |
| 47 | III / III | C | 1 | 47 | c.6449 G>A | p.Cys2150Tyr | ✓ | — | ✓ |
| 48 | III / III | A | 2 | Int. 38 | c.5461-10 T>C | Splice site | — | ✓ | — |
| | | | | 44 | c.6079 C>T | p.Leu2027Phe | — | ✓ | — |
| 49 | III / III | A | 1 | 12 | c.1721delAC | p.Asp574Aspfs*582 | ✓ | — | — |
| 50 | III / III | A | 1 | Int. 38 | c.5461-10 T>C | Splice site | — | ✓ | — |
| 51 | III / III | B | 2 | 35 | c.4918 C>T | p.Arg1640Trp | ✓ | — | — |
| | | | | 44 | c.6079 C>T | p.Leu2027Phe | ✓ | — | — |
| 52 | III / III | C | 1 | 22 | c.3323 G>A | p.Arg1108His | ✓ | — | — |
| 53 | III / III | A | 2 | Int. 38 | c.5461-10 T>C | Splice site | — | — | ✓ |
| | | | | 47 | c.6449 G>A | p.Cys2150Tyr | ✓ | — | ✓ |
| 54 | III / III | A | 2 | Int. 38 | c.5461-10 T>C | Splice site | — | — | ✓ |
| | | | | 47 | c.6449 G>A | p.Cys2150Tyr | ✓ | — | ✓ |
| 55 | III / III | A | 2 | Int. 38 | c.5461-10 T>C | Splice site | — | ✓ | ✓ |
| | | | | 47 | c.6449 G>A | p.Cys2150Tyr | — | ✓ | ✓ |
| 56 | III / III | D | 0 | | | | ✓ | — | — |
| 57 | III / III | A | 1 | **15** | **c.2239delC** | **p.Leu747Cysfs*787** | ✓ | — | ✓ |
| 58 | III / III | D | 0 | | | | ✓ | — | — |
| 59 | III / III | C | 1 | 5 | c.466 A>G | p.Ile156 Val | ✓ | — | — |

✓ = yes; — = no; APEX = arrayed primer extension microarray; BL = baseline; DS = Sanger direct sequencing; FU = follow-up; Int. = intron; SSCP = single-strand conformation polymorphism.

[a]Putative novel changes are in bold. All the variants are heterogeneous.

**SUPPLEMENTAL TABLE 7.** Investigation of the Pathogenicity of Identified *ABCA4* Variants

| Exon | Nucleotide Substitution and Amino Acid Change | Number of Alleles | Previous Report | SIFT[a] Pred. | SIFT[a] Index (0-1) | PolyPhen 2[a] Pred. | PolyPhen 2[a] Hum Var Score (0-1) | HSF Matrix[a] Site Affected | HSF Matrix[a] Wt CV | HSF Matrix[a] Mt CV | HSF Matrix[a] CV % Variation | Allelic Frequency Observed by EVS[a] | Reference |
|---|---|---|---|---|---|---|---|---|---|---|---|---|---|
| 3 | c.161 G>A, p.Cys54Tyr | 3 | Lewis[25] | Tol. | 0.11 | PRD | 0.994 | | | | No change | 1/10 758 | db SNP (rs150774447) |
| 3 | c.286 A>C, p.Asn96His | 1 | Papaioannou[26] | Tol. | 0.14 | PRD | 0.994 | | | | No change | 1/10 758 | db SNP (rs61748529) |
| 5 | c. 466 A>G, p. Ile156 Val | 2 | Papaioannou[26] | Tol. | 0.46 | Benign | 0.003 | | | | No change | 11/10 758 | db SNP (rs112467008) |
| 6 | c.768 G>T, p.Val256Val/Splice site | 1 | Klevering[24] | Tol. | 0.56 | NA | | Don. | 70.4 | 58 | Site broken (−17.51) | ND | |
| 9 | c.1222 C>T, p.Arg408* | 1 | Webster[29] | NA | | NA | | | | | | | |
| 10 | c.1253 T>C, p.Phe418Ser | 1 | Zernant[30] | Intol. | 0 | PRD | 0.99 | | | | No change | ND | |
| 10 | c.1317 G>A, p.Trp439* | 2 | This study | NA | | NA | | | | | | ND | |
| 12 | c.1721delAC, p.Asp574Aspfs*582 | 1 | Briggs[20] | NA | | NA | | Acc. | 47.2 | 68.3 | New site (44.5) | ND | |
| 14 | c.1957 C>T, p.Arg653Cys | 1 | Rivera[27] | Tol. | 0.1 | PRD | 0.999 | | | | No change | 1/10 758 | db SNP (rs141823837) |
| 14 | c.2023 G>A, p.Val675Ile | 1 | This study | Tol. | 0.07 | PRD | 0.989 | | | | NA | ND | |
| 15 | c.2239delC, p.Leu747Cysfs*787 | 1 | This study | NA | | NA | | Don. | 34.7 | 77 | New site (+122) | ND | |
| 17 | c.2588 G>C, p.Gly863Ala | 8 | Allikmets[11] | Intol. | 0.01 | PRD | 0.996 | | | | No change | 53/10 758 | db SNP (rs76157638) |
| 19 | c.2791 G>A, p.Val931Met | 1 | Allikmets[10] | Tol. | 0.12 | PRD | 0.716 | | | | No change | 18/10 758 | db SNP (rs58331765) |
| 19 | c.2828 G>A, p.Arg943Gln | 3 | Webster[29] | Intol. | 0.03 | Benign | 0.449 | Acc. | 52.2 | 81.1 | New site (+55.48) | 340/10 758 | db SNP (rs1801581) |
| 19 | c.2894 A>G, p.Asn965Ser | 1 | Lewis[25] | Intol. | 0 | PRD | 0.981 | Acc. | 53.4 | 82.3 | New site (+54.26) | ND | |
| 21 | c.3056 C>T, p.Thr1019Met | 2 | Rozet[28] | Intol. | 0 | PRD | 0.999 | | | | No change | ND | |
| 22 | c.3211_3212insGT, p.Ser1071Cysfs*1084 | 2 | Allikmets[10] | NA | | NA | | Don. | 69.3 | 28 | Site broken (−59.55) | ND | |
| 22 | c.3259 G>A, p.Glu1087Lys | 1 | Lewis[25] | Intol. | 0 | PRD | 0.997 | | | | No change | ND | |
| 22 | c.3322 C>T, p.Arg1108Cys | 2 | Rozet[28] | Intol. | 0 | PRD | 0.986 | | | | No change | 1/10 758 | db SNP (rs61750120) |
| 22 | c.3323 G>A, p.Arg1108His | 1 | Webster[29] | Intol. | 0 | PRD | 0.986 | | | | No change | ND | |
| 28 | c.4139 C>T, p.Pro1380Leu | 4 | Lewis[25] | Intol. | 0.01 | Benign | 0.377 | | | | No change | 2/10 758 | db SNP (rs61750130) |
| Int. 28 | c.4253+5 G>T, Splice site | 1 | Lewis[25] | NA | | NA | | Don. | 87.9 | 75.6 | Site broken (−14.02) | 1/10 758 | |
| 29 | c.4328 G>A, p.Arg1443His | 1 | Jaakson[23] | Tol. | 0.19 | PRD | 0.996 | | | | No change | ND | |
| 30 | c. 4363 C>T, p. Cys1455Arg | 1 | This study | Tol. | 0.34 | PRD | 0.994 | | | | NA | ND | |
| 30 | c.4469 G>A, p.Cys1490Tyr | 1 | Webster[29] | Intol. | 0.03 | PRD | 0.994 | | | | No change | ND | |
| 30 | c.4519 G>A, p.Gly1507Arg | 1 | This study | Tol. | 0.48 | PRD | 0.996 | Acc. | 78.9 | 78.9 | New site (+58.11) | ND | |
| 30 | c.4537_4538insC, p.Gly1513Profs*1554 | 1 | Briggs[20] | NA | | NA | | Acc. | 91.7 | 33.3 | Site broken (−63.76) | ND | |
| 35 | c.4918 C>T, p.Arg1640Trp | 1 | Rozet[28] | Intol. | 0 | PRD | 1 | | | | No change | ND | |
| 35 | c.4956 T>G, p.Tyr1652* | 1 | Fumagalli[22] | NA | | NA | | | | | | | |
| Int. 38 | c.5461-10 T>C | 9 | Briggs[20] | NA | | NA | | | | | | 3/10 758 | db SNP (rs1800728) |
| 39 | c. 5516 T>C, p. Phe1839Ser | 1 | This study | Intol. | 0 | PRD | 0.988 | | | | No change | ND | |
| Int. 40 | c.5714+5 G>A, Splice site | 1 | Cremers[13] | NA | | NA | | Donor | 85.5 | 73.3 | Wild-type site broken (−14.23) | ND | |
| 42 | c.5882 G>A, p.Gly1961Glu | 1 | Allikmets[11] | Tol. | 0.18 | PRD | 1 | | | | No change | 29/10 758 | db SNP (rs1800553) |

*Continued on next page*

**SUPPLEMENTAL TABLE 7.** Investigation of the Pathogenicity of Identified ABCA4 Variants (*Continued*)

| Exon | Nucleotide Substitution and Amino Acid Change | Number of Alleles | Previous Report | SIFT[a] Pred. | SIFT[a] Index (0-1) | PolyPhen 2[a] Pred. | PolyPhen 2[a] Hum Var Score (0-1) | HSF Matrix[a] Site Affected | HSF Matrix[a] Wt CV | HSF Matrix[a] Mt CV | HSF Matrix[a] CV % Variation | Allelic Frequency Observed by EVS[a] | Reference |
|---|---|---|---|---|---|---|---|---|---|---|---|---|---|
| 43 | c.5908 C>T, p.Leu1970Phe | 1 | Lewis[25] | Tol. | 0.14 | PRD | 0.997 | | | | No change | ND | |
| 44 | c.6079 C>T, p.Leu2027Phe | 4 | Allikmets[11] | Intol. | 0.02 | PRD | 0.999 | | | | No change | 3/10 758 | db SNP (rs61751408) |
| 44 | c.6089 G>A, p.Arg2030Gln | 2 | Lewis[25] | Tol. | 0.1 | PRD | 0.999 | | | | No change | 6/10 758 | db SNP (rs61750641) |
| 46 | c.6320 G>A, p.Arg2107His | 2 | Fishman[21] | Intol. | 0 | PRD | 0.996 | | | | NA | 83/10 758 | db SNP (rs62642564) |
| 47 | c.6449 G>A, p.Cys2150Tyr | 5 | Fishman[21] | Intol. | 0 | PRD | 0.995 | Don. | 76.6 | 49.8 | Site broken (−35.02) | 1/10 758 | db SNP (rs61751384) |

Acc. = acceptor site; Don. = donor site; EVS = Exome Variant Server; HSF = Human Splicing Finder program; Hum Var = Human Var score; Int. = intron; Intol. = intolerant; Mt CV = mutant consensus value; NA = not applicable; ND = not detected; PRD = probably damaging; Pred. = prediction; SIFT = Sorting Intolerant from Tolerance program; Tol. = tolerant; Wt CV = wild-type consensus value.

[a]SIFT (version 4.0.4) results are reported to be tolerant if tolerance index ≥ 0.05 or intolerant if tolerance index < 0.05. PolyPhen-2 (version 2.1) appraises mutations qualitatively as Benign, Possibly Damaging, or Probably Damaging based on the model's false-positive rate. The cDNA is numbered according to Ensembl transcript ID ENST00000370225, in which +1 is the A of the translation start codon. Human Splicing Finder (HSF, version 2.4.1) reports the results from the HSF matrix: the higher the consensus value (CV), the stronger the predicted splice site. The values for the wild-type and mutant sequences are shown; the larger the difference between these values, the greater the chance that the variant can affect splicing. EVS denotes variants in the Exome Variant Server, NHLBI Exome Sequencing Project, Seattle, WA, USA (accessed January 12, 2012; http://snp.gs.washington.edu/EVS/).

連載第1回

# 今さら聞けないQ&A

本連載は，眼科臨床または研究における素朴な疑問・初歩的な質問に，眼科専門医がわかりやすい解説を交えてお答えするコーナーです．また，本連載では質問案を随時受け付けております．巻末の読者アンケート用紙に聞いてみたい質問をご記入いただき，編集部までふるってご応募ください．

## Q1 OCTの「コストライン」について教えてください

**Answer**


**角田 和繁**

TSUNODA Kazushige

東京医療センター臨床研究センター（感覚器センター）視覚生理学研究室


### 1．COSTラインとは？

スペクトラルドメイン光干渉断層計（spectral domain-optical coherence tomography：SD-OCT）において後極部で観察される，視細胞層のIS/OSラインと網膜色素上皮層（retinal pigment epithelium：RPE）のあいだの高輝度の反射帯をcone outer segment tip（COST）ラインとよびます（図1A）．錐体視細胞外節の先端部は，RPEのmicrovilliによって包み込まれるような形態をしています．COSTラインに相当する解剖学的構造は外節の先端部（tip）であることが，Srinivasanら[1]の高解像度OCTによる観察によって示されています．一方，SpaideとCurcio[2]は過去の文献的データをもとにした解析により，錐体外節がmicrovilliによって包まれている領域全体（contact cylinder）がCOSTラインに相当すると強調しており，詳細な解剖学的位置関係についてはまだ議論の余地があるように思えます．

通常，COSTラインは中心窩ではRPEに接する位置にみられ，周辺部にいくほどその位置はIS/OSライン側（硝子体側）に移行していきます．これは錐体外節の長さが，中心窩から離れるほど短くなるためです．COSTラインは健常人において年齢にかかわらず確認することができますが[3]，後述するように測定上のさまざまな問題によって“false negative”となるので注意が必要です．

なお，杆体視細胞にも同様の構造は存在しており，固視の良好な被験者の黄斑部周囲にはrod outer segment tip（ROST）ラインとよばれる高輝度のラインが，COSTラインとRPEのあいだに観察されます[1]．

### 2．COSTラインが診断に役立つのはどのようなときか？

網膜外層疾患において，視細胞の機能的異常は細胞微細構造の変化と密接に結びついています．このため，COSTラインを観察することで，錐体視細胞の機能的異常を早期から検出することができます．この変化は通常IS/OSラインの変化に先行して生じるため，とくに視細胞の異常を検出するための鋭敏な視標として注目されているわけです[4)~6)]．

実際には，検眼鏡的所見や蛍光眼底造影所見が正常にもかかわらず視力が低下している患者さんにおいて，とくに威力を発揮します．その病態が網膜性であるか，あ

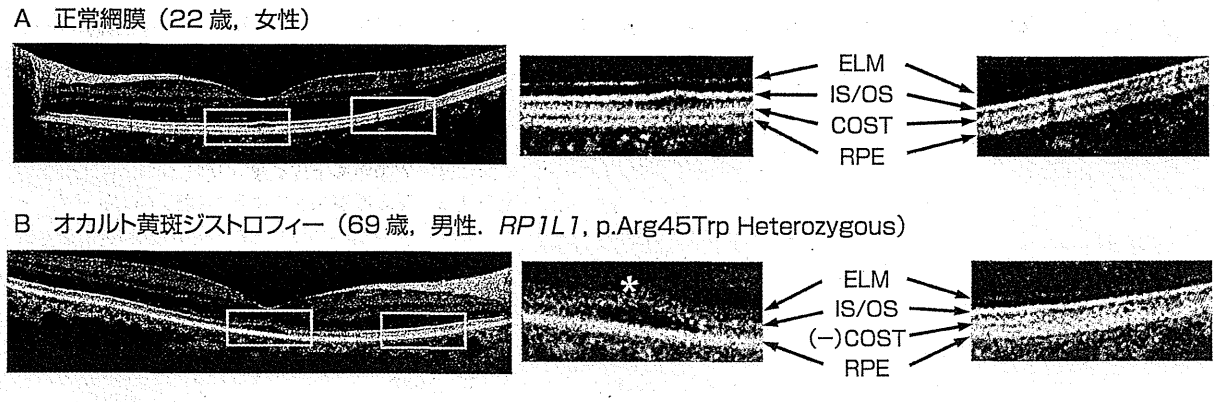


**図1 正常網膜（A），およびオカルト黄斑ジストロフィー（三宅病，*RP1L1* ヘテロ変異：p.Arg45Trp）（B）のOCT所見**

右に中心窩および周辺部の拡大図を示す．
オカルト黄斑ジストロフィーでは，COSTラインが中心窩において消失しているが，視機能の正常な鼻側網膜では正常に観察されている．また，中心窩のIS/OSラインは著しく不明瞭化している．

（Tsunoda K *et al*, 2012[5]より改変引用）

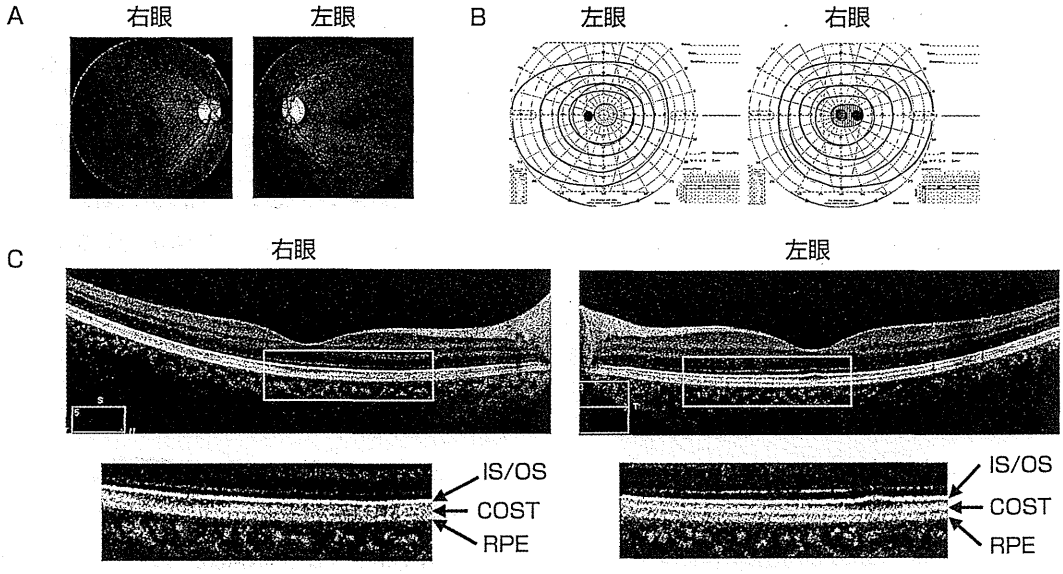


**図2 右眼AZOORの28歳女性．矯正視力，右（0.15），左（1.5）**

**A**：検眼鏡的所見は，左右ともに異常がみられない．
**B**：ゴールドマン視野にて，右眼にマリオット盲点の拡大および中心暗点を認める．
**C**：OCTでは，右眼の視野異常部位においてCOSTラインが不明瞭化している．一方，同部位のIS/OSラインは罹患眼でもほぼ正常に観察されている．

るいは視神経疾患，中枢性疾患によるものかを即座に鑑別できるばかりでなく，視細胞機能の低下している領域を二次元的に把握することもできます[4)5)]．網膜機能を評価するという意味では網膜電図（electroretinography：ERG）ほどの信頼性はありませんが，ERGに不慣れな眼科医が多い現在では，網膜外層疾患のスクリーニングとして大変重要です．

図1Bはオカルト黄斑ジストロフィー（三宅病，*RP1L1* ヘテロ変異：p.Arg45Trp）において，矯正視力が（0.1）まで低下した症例で，検眼鏡的所見，蛍光眼底造影所見はいずれも正常です．全視野ERGは正常ですが，黄斑部において局所的にERG反応が消失しています．OCTで観察すると，COSTラインが中心窩において消失しているものの，視機能の正常な鼻側網膜では正常に観察されることがわかります．また，中心窩のIS/OSラインは著しく不明瞭化しています．

表1　視細胞機能が正常にもかかわらずCOSTラインが消失，あるいは不明瞭化するケース

A）レーザー観察光が十分に網膜に届いていない場合
　・小瞳孔，角膜混濁，白内障，後発白内障，硝子体出血など．
B）レーザー観察光と視細胞層が垂直でない場合
　・視線と光軸とのズレ（α角）が大きいことによる眼球の光学的特性．網膜色素上皮剥離，網膜下出血，ドルーゼンなどによる網膜外層の局所的隆起．強膜・脈絡膜の肥厚，高度近視などによる後極部全体の形態変化．
C）網膜表層，あるいは網膜内に高反射部位が存在する場合
　・厚い黄斑前膜，網膜出血，硬性白斑など．
D）網膜内に著しい形態変化が生じている場合
　・黄斑円孔，網膜浮腫および嚢胞，黄斑前膜による網膜厚の増加，網膜分離など．
E）固視不良，眼球運動などのため，加算において画像のズレが生じている場合

図2はacute zonal occult outer retinopathy（AZOOR）によって矯正視力が（0.15）まで低下した症例で，検眼鏡的所見，蛍光眼底造影所見はいずれも正常です．中心窩において，局所的にERG反応が消失しています．OCTで観察すると，視野の異常部位においてCOSTラインが不明瞭化しています．なお，AZOORでは視野障害部位でIS/OSラインの異常がみられるのが一般的ですが，この症例では同部位のIS/OSラインはほぼ正常に観察されています．このことは，COSTラインがIS/OSラインにくらべてより鋭敏な視標であることを示しています．

また，網膜外層疾患のほかに黄斑円孔や黄斑前膜などにおいても，COSTラインと視力との関係が指摘されており，術後視機能の評価などに応用されています[7]．

## 3．COSTライン読影についての注意点

COSTラインは，たとえ視細胞機能が正常であってもさまざまな理由で描出されないことがあります．いわば「光学的に脆弱」な部位であり，診断にあたっては“false negative”の可能性をつねに念頭におく必要があります．

最も頻繁に問題となるのは，光量不足によってCOSTラインが消失するケースです．たとえばZeiss社製のHD-OCTにおいては取得画像のレーザー光量が「1から10」までのスケールで表示されますが，スケールが「8」を下回る場合には信頼性が低いため，筆者はCOSTラインの判定をおこなわないようにしています．

また，“false negative”の原因として見過ごされやすいのが，網膜面と光軸が垂直でないことによる信号の減衰です．COSTラインは外顆粒層のヘンレ層と同様，レーザー光の入射角に対する指向性が非常に高く，光が垂直に当たるときに最も輝度が高くなります[8]．実際には，描出画像において網膜面が水平から30度以上かたむいていると，COSTラインはほぼ消失してしまいます．これはレーザー光を瞳孔中心から左右にずらすことによって修正可能ですが，その分，網膜に届く光量自体が減少してしまうという問題が生じます．

その他，さまざまな光学的な問題点によってCOSTラインが消失，あるいは不明瞭化するケースを表1にあげました．このようなケースでは，たとえCOSTラインが明瞭に観察されなくても視細胞外節に異常があるとは断定できません．

## 4．IS/OS接合部の生理的機能について

最後にIS/OS接合部についてお答えします．当初は，視細胞内節と外節の境界部が強い干渉信号を出すことがOCTにおけるIS/OSラインの成因と考えられていました．近年，補償光学を組み合わせた高解像度OCTによる観察により，従来IS/OSラインとよばれていた部位は，視細胞内節のellipsoid（内節先端部の紡錘形の領域で，ミトコンドリアを多く含む）に相当することが確認されました[9]．

IS/OSラインが内節のellipsoidに相当すると考えると，臨床病態をよりうまく説明できる例を紹介します．オカルト黄斑ジストロフィーでは，早期からIS/OSラインの不明瞭化（膨潤化）が観察されます[5]．本疾患の原因となる*RP1L1*遺伝子は視細胞の構造維持に重要とされており，おもに視細胞内節に発現しています．このため中心窩付近のIS/OSラインに特徴的な膨潤化がみ

られると考えられます.

今後は，すでに一般化している「IS/OSライン」という呼称にかわって，たとえば「IS ellipsoidライン」などというよび方が一般化する可能性もあります．その点を網膜解剖学の権威であるCurcio教授に個人的にお聞きしたところ，彼女の意見は「もう少しみんなでデータを集めてから検討しましょう」というものでした．フーリエドメインOCTにおける各所見の解剖学的，病理学的対応関係は，技術の進歩によって今後さらに塗りかえられていく可能性があるかもしれません.

## 文 献


1) Srinivasan VJ *et al*：Characterization of outer retinal morphology with high-speed, ultrahigh-resolution optical coherence tomography. *Invest Ophthalmol Vis Sci* 49：1571-1579, 2008
2) Spaide RF *et al*：Anatomical correlates to the bands seen in the outer retina by optical coherence tomography：literature review and model. *Retina* 31：1609-1619, 2011
3) Rii T *et al*：Foveal cone outer segment tips line and disruption artifacts in spectral-domain optical coherence tomographic images of normal eyes. *Am J Ophthalmol* 153：524-529, 2012
4) Tsunoda K *et al*：Selective abnormality of cone outer segment tip line in acute zonal occult outer retinopathy as observed by spectral-domain optical coherence tomography. *Arch Ophthalmol* 129：1099-1101, 2011
5) Tsunoda K *et al*：Clinical characteristics of occult macular dystrophy in family with mutation of RP1l1 gene. *Retina* 32：1135-1147, 2012
6) Watanabe K *et al*：Outer retinal morphology and visual function in patients with idiopathic epiretinal membrane. *Arch Ophthalmol*, 2012 (in press)
7) Itoh Y *et al*：Correlation between length of foveal cone outer segment tips line defect and visual acuity after macular hole closure. *Ophthalmology* 119：1438-1446, 2012
8) Lujan BJ *et al*：Revealing Henle's fiber layer using spectral domain optical coherence tomography. *Invest Ophthalmol Vis Sci* 52：1486-1492, 2011
9) Fernandez EJ *et al*：Ultrahigh resolution optical coherence tomography and pancorrection for cellular imaging of the living human retina. *Opt Express* 16：11083-11094, 2008


# Q2 SNP解析のSNPとは何ですか？

## Answer


仲田 勇夫，山城 健児
NAKATA Isao, YAMASHIRO Kenji
京都大学大学院医学研究科感覚運動系外科学（眼科学）


SNPとは一塩基多型（single nucleotide polymorphism）のことで，遺伝的変化（遺伝子変異）の一種であり，一般的にDNA配列上の1つの塩基が異なる塩基に置きかわる塩基置換を指します．遺伝子変異には単一のDNA配列で起こる単純な突然変異や配列交換などさまざまなものが含まれますが，1人の個人に新たな変異が生じる確率は非常に低い（一塩基あたり約$2.5 \times 10^{-8}$）[1]といわれています．しかし，これらの変異が生殖細胞系列に起こり，そのまま子孫に伝達された場合，その変異が集団中の個体に広がり，結果的に同様の変異をもった集団が出現する場合があります．そして，ヒト集団のある遺伝子座に1%以上の頻度で生じている変異を“多型”とよび，一般的な遺伝子変異と区別してよばれます．近年における遺伝子型決定技術とその解析方法の発展はめざましいものがあり，多数のヒトに対して，遺伝子全体の網羅的なSNP解析（数十万～数百万SNPの同時解析）が全世界的に数多くおこなわれています．それに伴って新たなSNPも発見されつづけており，その総数は増えつづける一方です．たとえば，NCBI（The National Center for Biotechnology Information）の提供するdbSNP（http://www.ncbi.nlm.nih.gov/snp/）というデータベースでは，新たな実験・研究により発見されたSNPが

日々報告され，登録・更新されていますが，その数は2002年当初281万個だったものが，現在は435万個になっています．よくSNPをあらわすのにrs10490924などのrsナンバーが用いられることがありますが，これらは新たに報告されたSNP（ss#と名づけられます）の中で，公共データベース上で確認がとれたものに対して割りふられたIDであり（rsはreference SNPの略），その多型に固有のIDです．「わざわざそんなIDをふらなくても，場所がわかっているのだから何番染色体の何番目の塩基の多型といえばそれで済むじゃないか」と思われる方もいらっしゃるかもしれませんが，そのおおもととなる全遺伝子情報自体が更新されつづけているため（Genome Buildとよばれます．最新のものは2011年10月にリリースされたBuild 37.3），更新されても同じ多型を示すことを確実にするためにこのようなIDを使用しています．ただ，実際に一昔前まではc.205G>Tなどと特定の遺伝子座位から数えて何番目の変異という表記がSNPに対してもおこなわれていましたし，現在でもまれな変異や新たな変異などをあらわす際にはこのように表記する場合があります．ちなみに，塩基置換によって転写・翻訳を経た最終的な蛋白質のアミノ酸変化に注目してSNPを表記する場合もあり，その場合はA69S（69番目のアラニンがセリンに置換）などとあらわされます．

少し込み入った話になってしまいましたが，SNPを解析することにより，集団の遺伝的背景を知ることが容易になります．日本人の先祖はどこから来たかなど民俗学的な研究にも使用されたりするほかにも[2]，ある疾患の人たちにかたよって存在する多型を解析することによって病気の原因や本質を探ることに活用されています．加齢黄斑変性（age-related macular degeneration：AMD）は複数の遺伝子多型が発症に強く関与する疾患として有名ですが，遺伝子検査の結果を含めたさまざまな情報を組み合わせることにより，発症前からその危険予測ができる可能性が示唆されており，実際に欧米では遺伝子検査キットがすでに発売・実用化されています．一般にAMDなどの多因子疾患において発症に関与する遺伝子を“感受性遺伝子”とよび，メンデル遺伝病における“原因遺伝子”とは区別してよばれます．これは感受性遺伝子領域のSNPの頻度が疾患の頻度よりも非常に高く，あくまでも発症の危険度を上げるという役割のみをもっている，という意味で名づけられています．ただ，いまだ多くの多因子疾患においては，強い影響をもつSNPの発見は困難をきわめており，今後はSNP以外の他のさまざまな遺伝子変異にも注目が集まることになりそうです．

## 文献


1) Nachman MW *et al*：Estimate of the mutation rate per nucleotide in humans. *Genetics* **156**：297-304, 2000

2) Abdulla MA *et al*：Mapping human genetic diversity in Asia. *Science* **326**：1541-1545, 2009

OPEN ACCESS Freely available online

PLoS one

# Real-Time Imaging of Rabbit Retina with Retinal Degeneration by Using Spectral-Domain Optical Coherence Tomography

**Yuki Muraoka[1], Hanako Ohashi Ikeda[1]*, Noriko Nakano[1], Masanori Hangai[1], Yoshinobu Toda[2], Keiko Okamoto-Furuta[2], Haruyasu Kohda[2], Mineo Kondo[3], Hiroko Terasaki[4], Akira Kakizuka[5], Nagahisa Yoshimura[1]**

**1** Department of Ophthalmology and Visual Sciences, Kyoto University Graduate School of Medicine, Kyoto, Japan, **2** Center for Anatomical Studies, Kyoto University Graduate School of Medicine, Kyoto, Japan, **3** Department of Ophthalmology, Mie University School of Medicine, Tsu, Japan, **4** Department of Ophthalmology, Nagoya University Graduate School of Medicine, Nagoya, Japan, **5** Laboratory of Functional Biology, Kyoto University Graduate School of Biostudies and Solution Oriented Research for Science and Technology, Kyoto, Japan

## Abstract

*Background:* Recently, a transgenic rabbit with rhodopsin Pro 347 Leu mutation was generated as a model of retinitis pigmentosa (RP), which is characterized by a gradual loss of vision due to photoreceptor degeneration. The purpose of the current study is to noninvasively visualize and assess time-dependent changes in the retinal structures of a rabbit model of retinal degeneration by using speckle noise-reduced spectral-domain optical coherence tomography (SD-OCT).

*Methodology/Principal Findings:* Wild type (WT) and RP rabbits (aged 4–20 weeks) were investigated using SD-OCT. The total retinal thickness in RP rabbits decreased with age. The thickness of the outer nuclear layer (ONL) and between the external limiting membrane and Bruch's membrane (ELM–BM) were reduced in RP rabbits around the visual streak, compared to WT rabbits even at 4 weeks of age, and the differences increased with age. However, inner nuclear layer (INL) thickness in RP rabbits did not differ from that of WT during the observation period. The ganglion cell complex (GCC) thickness in RP rabbits increased near the optic nerve head but not around the visual streak in the later stages of the observation period. Hyper-reflective change was widely observed in the inner segments (IS) and outer segments (OS) of the photoreceptors in the OCT images of RP rabbits. Ultrastructural findings in RP retinas included the appearance of small rhodopsin-containing vesicles scattered in the extracellular space around the photoreceptors.

*Conclusions/Significance:* In the current study, SD-OCT provided the pattern of photoreceptor degeneration in RP rabbits and the longitudinal changes in each retinal layer through the evaluation of identical areas over time. The time-dependent changes in the retinal structure of RP rabbits showed regional and time-stage variations. *In vivo* imaging of RP rabbit retinas by using SD-OCT is a powerful method for characterizing disease dynamics and for assessing the therapeutic effects of experimental interventions.

**Citation:** Muraoka Y, Ikeda HO, Nakano N, Hangai M, Toda Y, et al. (2012) Real-Time Imaging of Rabbit Retina with Retinal Degeneration by Using Spectral-Domain Optical Coherence Tomography. PLoS ONE 7(4): e36135. doi:10.1371/journal.pone.0036135

**Editor:** Steven Barnes, Dalhousie University, Canada

**Received** November 27, 2011; **Accepted** March 26, 2012; **Published** April 27, 2012



**Funding:** This research was supported by Research grants from the Astellas Foundation for Research on Metabolic Disorders and the Japan Foundation for Applied Enzymology, and a Grant-in-Aid for Young Scientists (22791656) from the Ministry of Education, Culture, Sports, Science and Technology (MEXT). The funders had no role in study design, data collection and analysis, decision to publish, or preparation of the manuscript.

**Competing Interests:** The authors have declared that no competing interests exist.

* E-mail: hanakoi@kuhp.kyoto-u.ac.jp

## Introduction

Retinitis pigmentosa (RP) is an inherited retinal disorder characterized by a progressive loss of visual function due to degeneration of rod and cone photoreceptors and eventual atrophy of the entire retina [1,2]. However, there are no effective treatments for RP. Various animal models of RP have been developed and studied to elucidate the pathophysiology of the disease and to develop new treatments [3–10]. Of these models, only monkeys have a macula, an important area for vision due to the high density of cone photoreceptors. However, it is not easy to study the pathophysiology of RP in monkeys due to handling and breeding difficulties. Rabbits are known to have a visual streak, where the rod and cone photoreceptor density is highest, about 3 mm ventral to the optic nerve head (ONH) [11,12]. Rabbits are easy to breed and handle, and the physiology and morphology of rabbit retina is well understood [11–14]. Additionally, in mid-sized animals like rabbits, surgical treatments such as subretinal injection of cells for regenerative therapy [15,16], vectors for gene therapy [17], and implantation of intraocular devices [18,19] are easily performed. Therefore, rabbits are very useful for studying retinal diseases and testing new therapeutic interventions. For these reasons, we used transgenic (Tg) rabbits with mutated rhodopsin (Pro 347 Leu, RP rabbits) as a mid-sized model for RP

[20] to study the pathophysiology and develop new evaluation systems for retinal degeneration.

Optical coherence tomography (OCT) devices allow non-invasive detection of retinal architecture, including quantitative measurements of retinal thickness and longitudinal observation of the retinal architecture [21]. The technological advances in spectral-domain OCT (SD-OCT) have enabled high-speed scanning and improved image resolution [22]. Furthermore, the exact averaging of B-scans with a three-dimensional eye-tracking system and high-speed scanning have enabled sufficient reduction in speckle noise, the most influential artificial noise that blurs the boundaries between retinal layers [23,24]. These advances have improved visualization of individual retinal layers, including both the outer retina and the inner retina (i.e., ganglion cell layer and inner plexiform layer [IPL] in humans) [25,26]. SD-OCT imaging also enables evaluation of the junction between the inner segment (IS) and the outer segment (OS) of the photoreceptors (IS/OS) [27–29] and that of the external limiting membrane (ELM) [30,31] as hallmarks of photoreceptor integrity. That is, visual function can be speculated from OCT images to some extent. Thus, the use of OCT imaging in humans has contributed to a more detailed understanding of the pathophysiology of many retinal diseases. In mice, the retina has been clearly visualized using SD-OCT [32–37]. Thus, in experimental animals, SD-OCT may allow *in vivo* detection and monitoring of changes in retinal architecture without sacrificing animals.

In mouse models of retinal degeneration, Fischer [36] and Huber et al. [32] detected and analyzed photoreceptor degeneration by using SD-OCT. They imaged the thinning of inner retinal layers and compared the total retinal thickness with that of normal mice in several mouse RP models. Yamauchi et al. reported the retinal architecture of rabbits by using SD-OCT following iodoacetic acid-induced photoreceptor degeneration [38]. However, retinal pathomorphology of genetically engineered rabbit models of RP, which mimic human RP [20], and longitudinal assessment of changes in the individual retinas remain to be studied with SD-OCT.

The purpose of this study was to visualize the time-dependent changes in photoreceptors, elucidate the pattern of changes in each retinal layer around the visual streak in identical eyes of RP rabbits by using SD-OCT, and assess the visual functions by electroretinography (ERG).

## Results

### Visualization of retinal structures in RP rabbits with SD-OCT

We first investigated whether the retinal structures of WT rabbits could be clearly visualized using SD-OCT. Vertical OCT images, which passed through the center of the ONH (Fig. 1A), permitted clear identification of each retinal layer, the choroid, and sclera of WT rabbits (Figs. 1B and 1C). The ELM and IS/OS lines were also clearly identifiable, the integrity of which have been shown to be positively associated with visual function. In the vertical OCT images, the scleral ring was defined as the edge of the ONH so that OCT measurements could be longitudinally compared between each rabbit and between WT and RP rabbits (Fig. 1B).

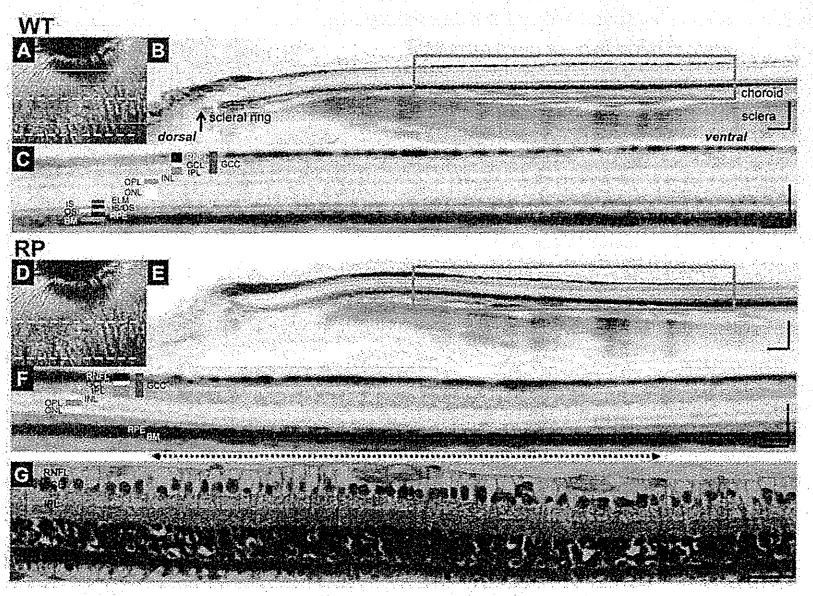


**Figure 1. SD-OCT images of WT and Retinitis Pigmentosa (RP) rabbit retinas and histology of the visual streak in an RP rabbit.** (A) A fundus infrared image of a WT rabbit retina, including optic nerve head (ONH) and visual streak. The area between dotted lines is the visual streak. (B) A vertical SD-OCT image along the green arrow in panel A, which passes through the center of the ONH. On this vertical image, the scleral ring was regarded as the lower margin of the ONH. (C) A magnified OCT image of the area enclosed by the blue square in panel B, which includes the visual streak. (D) A fundus infrared image of a RP rabbit retina, including the ONH and visual streak. (E) A vertical SD-OCT image of a 20-week-old RP rabbit along the green arrow in panel D. (F) A magnified OCT image of the area enclosed by the blue square in panel E. The 2.2 mm width of this OCT section was vertically cut between 1.8 mm and 4.0 mm ventral to the inferior edge of the ONH. A dotted arrow indicates the region of the visual streak. (G) Hematoxylin-Eosin staining of a retinal section corresponding to the area in the OCT image in F. Scale Bar = 200 μm (B, E), 100 μm (C, F), and 50 μm (G). RNFL, retinal nerve fiber layer; GCL, ganglion cell layer; IPL, inner plexiform layer; GCC, ganglion cell complex; INL, inner nuclear layer; OPL, outer plexiform layer; ONL, outer nuclear layer; ELM, external limiting membrane; IS, inner segments of photoreceptors; OS, outer segments of photoreceptors; IS/OS, junctions between IS and OS; RPE, retinal pigment epithelium; and BM, Bruch's membrane.
doi:10.1371/journal.pone.0036135.g001

Next, we examined a 20-week-old RP rabbit that expressed mutated rhodopsin (Figs. 1D–1F). The outer nuclear layer (ONL) of the RP rabbit was much thinner than the WT rabbit. Furthermore, in the RP rabbit, the photoreceptors around the visual streak (indicated by the dotted arrow), where the densities of rod and cone photoreceptors were the highest, appeared to be more severely damaged than in any other area. In this area, the ONL was very thin and the outer plexiform layer (OPL) was faint or absent depending on the distance from the ONH and the IS/OS line was undetectable (Fig. 1F). This regional variation in photoreceptor damage was also detected with hematoxylin and eosin (H&E) staining in the same eye (Fig. 1G).

## Time-dependent changes in the photoreceptor layers and in the visual function of RP rabbits

As observations revealed that photoreceptor damage was severe around the visual streak, we were encouraged to investigate the time-dependent changes in the photoreceptors of identical RP rabbits beneath the visual streak with SD-OCT and compared them with those of the WT rabbits (Fig. 2A). At 4 weeks of age (with the youngest that can be examined by OCT), the ONL of RP rabbits was almost as thick as WT rabbits. Following 4 weeks of age, the ONL thickness in RP rabbits decreased. At 20 weeks, the ONL thickness in RP rabbits was much smaller than in WT rabbits. Photoreceptor IS and OS, where visual phototransduction occurs, were thin in RP rabbits. In contrast, the architecture of the inner retina was relatively preserved in RP rabbits at both 10 and 20 weeks of age.

In the current SD-OCT study, there were additional findings in the photoreceptor layers. In the sections of WT rabbits, the reflectivity of IS and OS was low compared to that of the ELM and IS/OS lines. In contrast, the IS and OS were highly reflective in RP rabbits, and almost equivalent to the ELM and IS/OS lines throughout the study ages (Fig. 2A).

To compare the SD-OCT data with those from the histological examination, histological sections of the age-matched RP and WT rabbits were prepared (Fig. 2B). The number of photoreceptors and thickness of the ONL, IS, and OS in the RP rabbits decreased with age, which is consistent with those of a previous report [20]. At 20 weeks of age, the nuclei of photoreceptors in RP rabbits were reduced to 1 or 2 rows, which was much less compared to WT rabbits. The magnitude of the decrease in ONL thickness appears similar between the histological and SD-OCT data (Figs. 2A and 2B). In the histological sections of a 4-week-old RP rabbit, the total retinal thickness and the ONL thickness were almost the same as those of the WT rabbit, and the IS and OS appeared intact. The high reflectivity in the IS and OS observed in the OCT sections was difficult to explain by the histological sections (Figs. 2A and 2B).

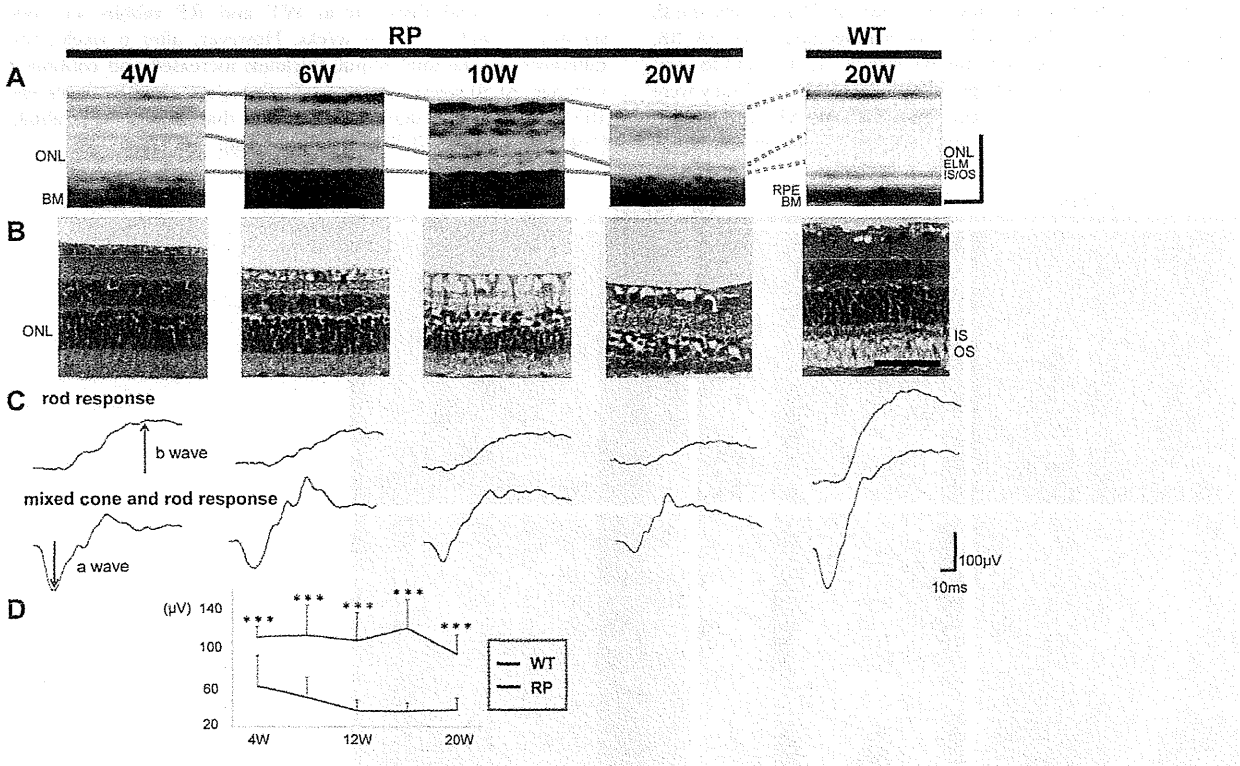


**Figure 2. Time-dependent changes in morphological features of the retina and visual function in the RP rabbits.** (A) SD-OCT images beneath the visual streak in an RP rabbit at 4, 6, 10, and 20 weeks and in a 20-week-old WT rabbit. The total retinal and ONL thickness in the RP rabbits decreased with age. The IS and OS were highly reflective in the RP rabbits compared with the WT rabbits. ONL, outer nuclear layer; and OS, outer segments of photoreceptors. (B) Hematoxylin-eosin staining of retinas in 4-, 6-, 10-, and 20-week-old RP and 20-week-old WT rabbits. The ONL in RP rabbits thinned with age. In 20-week-old RP rabbits, only 1–2 layers of nuclei were detected in the ONL. (C) Representative scotopic electroretinograms of 4-, 6-, 10-, and 20-week-old RP and 20-week-old WT rabbits. (D) The a-wave amplitude of the mixed rod and cone response. The amplitude was smaller in the RP rabbits than in the WT rabbits. The differences between the WT and RP rabbits were significant at all study points between 4 and 20 weeks. $^{*}P<0.05$, $^{***}P<0.001$ (unpaired $t$-test). Scale Bar = 100 μm in A, and 50 μm in B. ONL, outer nuclear layer; ELM, external limiting membrane; IS/OS, junctions between inner segment (IS) and outer segment (OS); RPE, retinal pigment epithelium; and BM, Bruch's membrane.

doi:10.1371/journal.pone.0036135.g002

Next, to evaluate visual function of the rod and cone systems of RP rabbits, scotopic full-field ERG was recorded (Fig. 2C). The a-wave of the mixed cone and rod response, which mainly originates from the photoreceptors, was smaller in RP rabbits (61.2±30.5 μV) (mean ± SD) than in WT rabbits (110.3±10.7 μV; $P=0.010$, unpaired $t$-test) as early as 4 weeks. The a-wave amplitude was reduced with RP rabbit aged (Fig. 2D). At the age of 20 weeks, the a-wave amplitude decreased to 37.6±11.5 μV in RP rabbits and was significantly less than that of WT rabbits (93.5±19.0 μV; $P<0.001$, unpaired $t$-test, Figs. 2C and 2D). The b-wave amplitude of the rod response, which originates indirectly from bipolar and Müller cells, was 97.3±33.2 μV in RP rabbits and was less than that of WT rabbits (280.8±71.3 μV; $P<0.001$, unpaired $t$-test, Fig. 2C). These data suggest that the visual function of both the rod and cone systems was disturbed in RP rabbits, consistent with a previous report [20]. These results indicate that loss of photoreceptors and concomitant visual dysfunction gradually occurs in RP rabbits.

## Vesicles cleaved from photoreceptors and disorganization of IS and OS in RP rabbits account for the hyper-reflectivity seen in SD-OCT images

To elucidate the cause of the hyper-reflective change in the outer photoreceptor layers of RP rabbits in SD-OCT sections, we examined and compared the ultrastructure of the retina between RP and WT rabbits at 4 or 20 weeks of age. In WT rabbits, the IS and OS exhibited a dense and regular arrangement (Figs. 3A, 3B, S1A and S1B). In contrast, in the RP retinas, the IS and OS were less organized at 4 weeks of age (Figs. 3C and 3D), and they were mostly absent at 20 weeks of age (Figs. S1C and S1D). Magnified images of the RP retinas revealed large number of small, approximately 100 nm, vesicles scattered in the extracellular space around the photoreceptors (arrowheads in Fig. 3D and S1D). These small vesicles appeared to be cleaved from the membrane of the IS in RP rabbits (arrows in Fig. 3E and S1D).The disrupted organization and the presence of vesicles between the IS and OS on ultra microscopy may account for the hyper-reflectivity seen in the corresponding area of the SD-OCT images.

To determine the origin of the vesicles, we performed ultrastructural immunohistochemistry by using monoclonal antibodies against rhodopsin (Fig. 3F). In RP retinas, numerous vesicles with dots were observed, indicating the presence of rhodopsin within the vesicles (disintermediated arrowheads in Fig. 3F).

## Time-dependent changes in the individual retinal layers in SD-OCT sections exhibit regional and time-stage variations in RP rabbits

In the SD-OCT examinations, the retinal thickness in the RP rabbits appeared to decrease with age. Therefore, we quantitatively measured the mean total retinal thickness around the visual streak in the WT and RP rabbits (Figs. 4A and S2). As shown in Fig. 4A, the total retinal thickness in WT rabbits did not change with age, whereas that of the RP rabbits progressively decreased. The total retinal thickness in WT and RP rabbits was not significantly different at 4 weeks. However, after 6 weeks, the differences in the total retinal thickness increased and continued with age. At 20 weeks, the total retinal thickness in RP rabbits was 165.8±8.5 μm and significantly smaller than that of WT rabbits (194.3±7.7 μm; $P<0.001$, unpaired $t$-test).

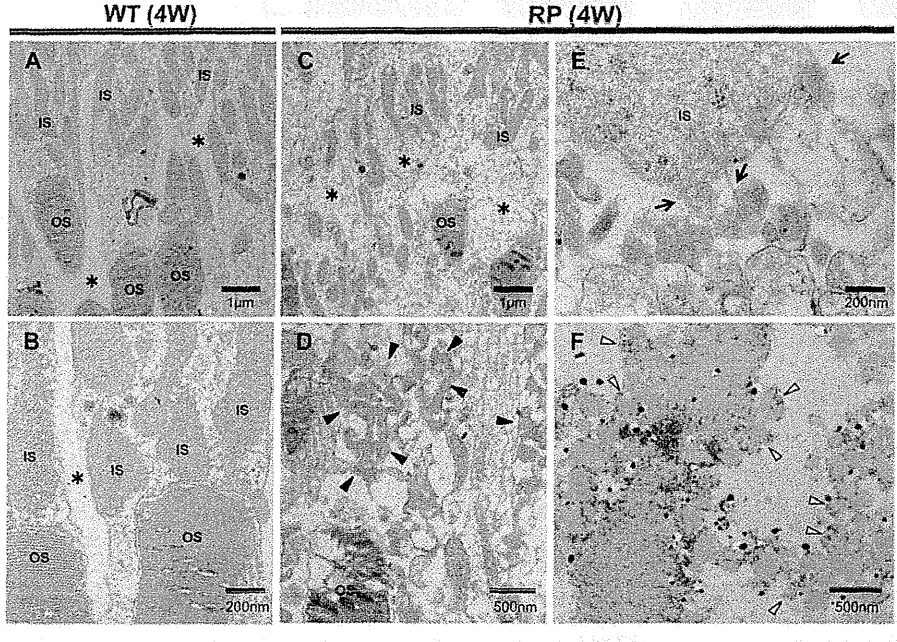


**Figure 3. Ultrastructure of photoreceptors in WT and RP rabbits.** (A, B) Ultrastructure of photoreceptors in 4-week-old WT rabbits. The inner (IS) and outer segments (OS) of the photoreceptors were regular and dense. There are no vesicles in the extracellular spaces (*). (C–E) Ultrastructure of the photoreceptors in the 4-week-old RP rabbits. The IS and OS were less organized than those in the WT rabbits. In the magnified image (D), the RP rabbit retina showing many small vesicles (arrowheads) accumulated in the extracellular spaces (indicated with * in panel C). The vesicles appeared to be cleaved from the IS into the extracellular space around the photoreceptors (arrows in panel E). (F) Ultrastructural immunohistochemistry by using an anti-rhodopsin antibody. The small vesicles (disintermediated arrowheads) in the extracellular spaces around the photoreceptors exhibit black dots indicating the presence of rhodopsin.
doi:10.1371/journal.pone.0036135.g003

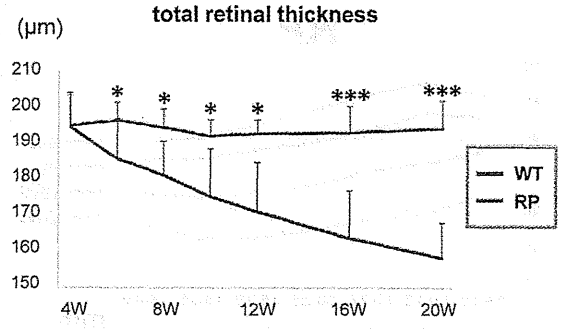


**Figure 4. Time-dependent changes in total retinal thickness, and mixed cone and rod response in the WT and RP rabbits.** The total retinal thicknesswas measured within a circle 1 mm in diameter 3 mm ventral to the lower margin of the ONH and averaged. The total retinal thickness in the WT rabbits (indicated with a blue line) was unchanged during observation, whereas that in the RP rabbits (indicated with a red line) severely decreased with age. *$P<0.05$, ***$P<0.001$ (unpaired *t*-test).
doi:10.1371/journal.pone.0036135.g004

OCT examination showed that the photoreceptors were most severely damaged at the visual streak, approximately 3 mm ventral to the ONH [11]. Therefore, we longitudinally examined regional and periodical variations in the progression of retinal degeneration in RP rabbits. For this purpose, we measured the thickness of each retinal layer within 0.5-mm areas 4 mm ventral to the lower edge of the ONH as a function of distance from the lower optic disc margin at 4, 6, 10, and 20 weeks by using the vertical OCT images that passed through the center of the ONH and visual streaks (Fig. S3).

**ONL thickness.** We first evaluated the thickness of the ONL where the nuclei of photoreceptors are located (Fig. 5A). In WT rabbits, the ONL in each area became slightly thinner with age. In younger WT rabbits (4–6 weeks old), the ONL was thinner in areas more distant from the ONH. In RP rabbits, the decrease in ONL thickness with age was more progressive than that of WT rabbits. At any age examined, thinning of the ONL was greater in areas more distant from the ONH. At 10 and 20 weeks, the ONL was thinnest in the area 3.0–3.5 mm ventral to the ONH.

At 4 weeks, the ONL thickness in RP rabbits was significantly less than that of WT rabbits in only the area 3.0–3.5 mm from the ONH ($P = 0.037$, unpaired *t*-test). Areas that exhibited a difference in ONL thickness between WT and RP rabbits expanded with age. At 20 weeks, the ONL thickness in RP rabbits was significantly smaller than that of WT rabbits in each of the 7 areas examined ($P<0.001$, unpaired *t*-test, Fig. 5E).

**ELM–BM thickness.** The ELM–BM thickness was evaluated because the area between the ELM and BM includes the length of the IS and OS where visual phototransduction occurs (Figs. 5B and S3). In WT rabbits, the ELM–BM thickness was larger in areas more distant from the ONH at any age examined. On the other hand, in RP rabbits, the differences in the ELM–BM thickness between areas as a function of distance from the ONH were smaller compared to those of WT rabbits at 4–10 weeks; the ELM–BM thickness appeared to decrease mainly in the areas distant from the optic disc. In 20-week-old RP rabbits, the ELM–BM thickness markedly decreased in the area 2.5–3.5 mm ventral to the ONH and was significantly less than that in the corresponding areas in WT rabbits ($P<0.001$, unpaired *t*-test, Fig. 5E).

**INL thickness.** The INL comprises the nuclei of bipolar, horizontal, amacrine, and Müller cells. The INL thickness was larger in areas more distant from the ONH in both WT and RP rabbits at the ages of 4 to 20 weeks (Fig. 5C). The INL thickness in WT and RP rabbits was not significantly different in each corresponding area at all the ages examined (Fig. 5E).

**GCC thickness.** The GCC consists of the retinal nerve fiber layer (axons of ganglion cells), ganglion cell layer (somas of ganglion cells), and IPL. To determine the influence of photoreceptor degeneration on the inner retina, GCC thickness was measured (Figs. S3 and 5D). The GCC thickness in the WT and RP rabbits exhibited a similar pattern in all the areas examined at the ages of 4 and 6 weeks. However, in 20-week-old RP rabbits, the GCC thickness in the areas close to the ONH was larger than in younger RP rabbits and in the corresponding areas of 20-week-old WT rabbits ($P<0.001$ for both, unpaired *t*-test, Fig. 5E).

In summary, the decrease in the ONL and ELM–BM thickness in RP rabbits was first detected in the areas approximately 3.0 mm ventral to the lower edge of the ONH (areas corresponding to the visual streak). Thinning of the IS and OS (measured as the ELM–BM thickness) followed thinning of the ONL. In contrast, the INL thickness in RP rabbits did not change throughout the observational period of 4 to 20 weeks. The GCC thickness in RP rabbits increased in areas away from the visual streaks but close to the ONH in the later phase of observation (Fig. 5E).

## Discussion

In this study, we examined time-dependent changes in photoreceptor degeneration in identical RP rabbits, and compared the pattern of changes in individual retinal layers between WT and RP rabbits for the first time by using SD-OCT. In RP rabbits, we observed regional differences in the degree of photoreceptor loss. That is, the ONL (ONL: the somas of photoreceptors) in RP rabbits was thinnest beneath the visual streak, where the densities of rod and cone photoreceptors were the highest in WT rabbits, and the photoreceptors of RP rabbits were relatively preserved in the area near the ONH. The current observations by using SD-OCT revealed longitudinal changes in the RP rabbit retina that were fairly consistent with a previous histological study of the RP rabbits [20] and reports based on other animal models of RP [3,9].

To elucidate the unique "highly reflective IS and OS" feature of the outer photoreceptor layer during photoreceptor degeneration in RP rabbits, an electron microscopy study was conducted on 4- or 20-week-old RP rabbits. We detected vesicles around the photoreceptors and loss of most of the IS and OS. We speculate that these destructive structures in RP rabbits cause the hyper-reflectivity seen in the outer photoreceptor layers (between ELM and BM) on SD-OCT images (Fig. 2A).The vesicles appeared to be cleaved from the IS, as described in a previous report [20]. Moreover, these vesicles were shown to include rhodopsin by ultrastructural immunohistochemistry (Fig. 3F), indicating that the particles were derived from photoreceptors. In SD-OCT images of 4-week-old RP rabbits, the area between the ELM and BM was hyper-reflective even though the reflectivity and the thickness of the ONL were unchanged (Fig. 2A). These observations point to the mechanism by which photoreceptors degenerate in RP rabbits. That is, defective transport of rhodopsin from the IS to the OS, which was demonstrated in mice with mutated rhodopsin P347S by using an antibody against the mutated rhodopsin [39], is followed by cleavage of vesicles from the IS, and finally cell bodies of photoreceptors degenerate. It is speculated that early stage RP patients may have mutations in the rhodopsin gene if hyper-reflective patterns are detected with SD-OCT in the area corresponding to the IS and OS, though further studies are needed to confirm this speculation.

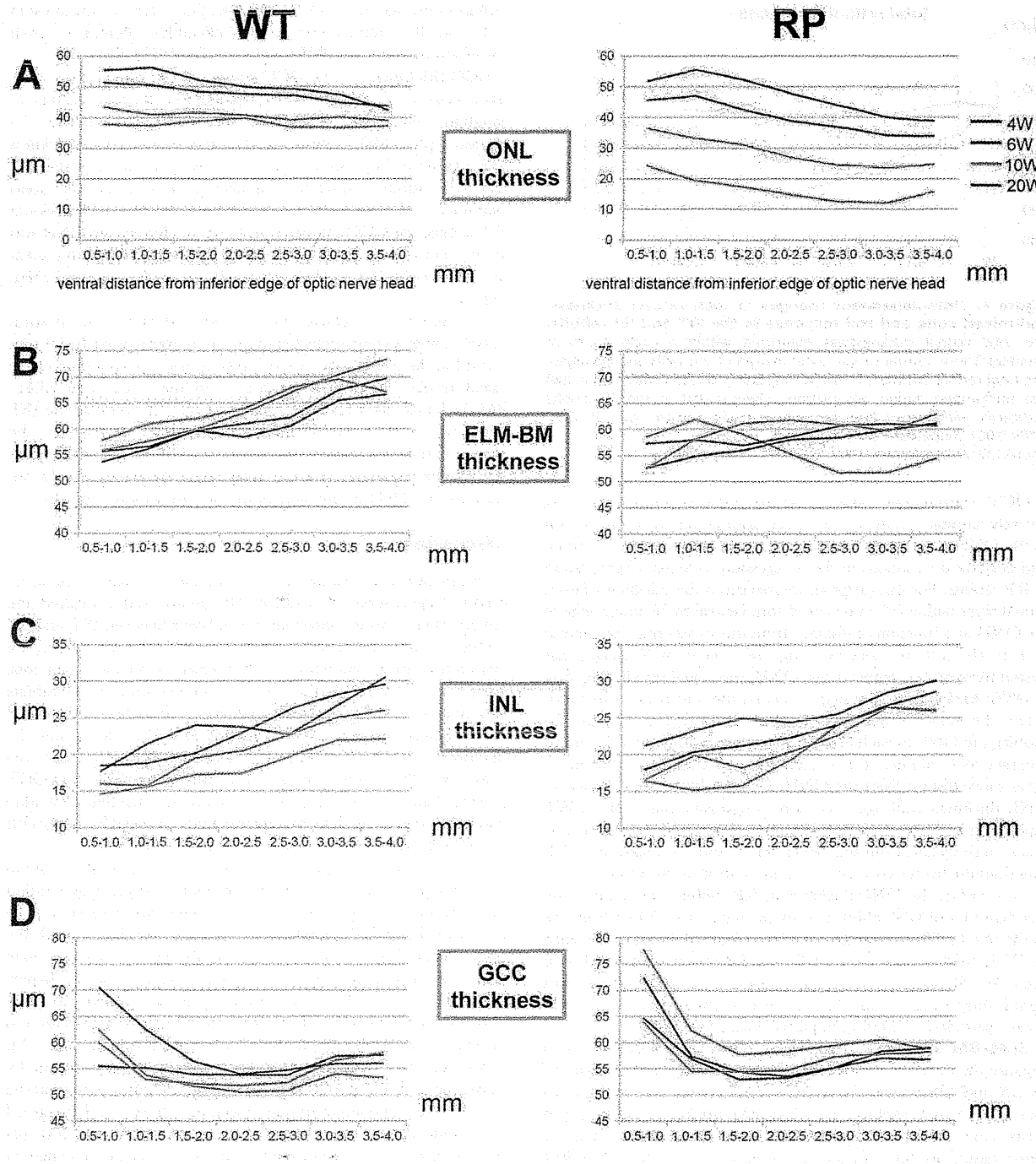
WT
RP
A
ONL thickness
μm
mm
ventral distance from inferior edge of optic nerve head
4W
6W
10W
20W
B
ELM-BM thickness
C
INL thickness
D
GCC thickness
E
ONL
ELM-BM
INL
GCC
0.5-1.0 1.0-1.5 1.5-2.0 2.0-2.5 2.5-3.0 3.0-3.5 3.5-4.0

**Figure 5. Time-dependent changes in the thickness of individual retinal layers in WT and RP rabbits.** (A–D) Time-dependent changes in ONL (A), ELM–BM (B), INL (C), and GCC (D) thickness measured with vertical OCT sections of WT and RP rabbits. Mean values at 4, 6, 10, and 20 weeks are indicated with blue, red, green, and purple lines, respectively. X-axes indicate the distance from the inferior edge of the ONH. (E) A schema to show time course and regional variations in the thickness of each retinal layer in RP rabbits from 4 to 20 weeks. Blue color indicates the regions where retinal thickness of RP rabbits was significantly smaller than that of WT rabbits. Orange color indicates the regions where retinal thickness of RP rabbits was significantly larger than that of WT rabbits. Deep and light colors indicate $P<0.001$ and $P<0.05$, respectively (unpaired *t*-test). ONL, outer nuclear layer; ELM, external limiting membrane; BM, Bruch's membrane; INL, inner nuclear layer; and GCC, ganglion cell complex.
doi:10.1371/journal.pone.0036135.g005

Aleman et al. reported the following disease sequence in human and murine RP caused by mutation of the rhodopsin gene: ONL diminution with INL thickening, amalgamation of residual ONL with the thickened INL, and progressive retinal remodeling with eventual thinning seen in OCT [40]. In our SD-OCT study, the INL thickness was not significantly different between WT and RP rabbits at the ages of 4 to 20 weeks. In contrast, the GCC thickness in RP rabbits paradoxically increased in the later phase of observation. Previous studies have suggested that the increase in the INL/inner retinal thickness in patients with RP maybe related to Müller glial activation with hypertrophy [40–42]. In the current study with RP rabbits, the observational period may be too short to detect an increase in INL thickness, or the gliosis of Müller cells may occur preferably within the GCC than in the INL.

This study has some limitations. The area imaged with SD-OCT was quite restricted such that the degeneration in RP retinas obtained with SD-OCT did not always correlate with the total retinal function. Furthermore, OCT or ERG could not be performed on rabbits younger than 4 weeks as their eyelids had not yet opened.

In conclusion, despite these short comings, *in vivo* time-dependent changes in the retinal structures were seen layer-by-layer in RP rabbits by using SD-OCT. These changes in the retinal structure had regional and temporal variations not only in the outer retina but also in the inner retina of RP rabbits. This study demonstrates that *in vivo* imaging with SD-OCT can facilitate the characterization of morphological disease dynamics and serve as a powerful tool for developing new treatments, such as gene therapy, intraocular devices, and neuroprotective treatments, in rabbit models of RP.

## Methods

### Experimental animals

This study was conducted in accordance with the Association Research in Vision and Ophthalmology (ARVO) Statement for the Use of Animals in Ophthalmic and Vision Research. All the protocols were approved by the Institutional Review Board of the Kyoto University Graduate School of Medicine (MedKyo11229).

New Zealand White rabbits (NZW, WT) and RP rabbits with rhodopsin P347L mutation (NZW, RP) [20] were purchased from Kitayama Labes Co., Ltd (Ina, Nagano, Japan). All rabbits were kept under a 14 h–10 h light-dark cycle (approximately 200 lux), given free access to water, and fed once a day. For the ERG recording and SD-OCT image acquisition, male WT (n = 4–10 eyes) and RP rabbits (n = 10–16 eyes) were used.

### Retinal histology

Rabbit eyes were fixed overnight in a mixture of 10% neutral buffered formalin and 2.5% glutaraldehyde and then transferred to 10% neutral buffered formalin. The tissues were trimmed, embedded in paraffin, sectioned vertically through the optic nerve (superior-inferior), and stained with hematoxylin and eosin. The retina beneath the visual streak was examined and compared between 10- and 20-week-old WT and RP rabbits.

### ERG

ERG was performed to assess the visual function of WT and RP rabbits at 4, 6, 10, and 20 weeks. Pupils were dilated with tropicamide (0.5%) and phenylephrine (0.5%) eye drops. Rabbits were dark-adapted for more than 60 min before anesthetization with an intramuscular injection of ketamine (25 mg/kg) and xylazine (2 mg/kg). ERG was recorded using a gold loop corneal electrode with a light-emitting diode (Mayo Corp., Inazawa, Japan). A reference electrode was placed in the mouth, and a ground electrode was attached to the ear. Stimuli were produced with a light-emitting diode stimulator (Mayo Corp.). The ERG response signals were amplified, digitized at 10 kHz with a band-pass filter of 0.3 to 500 Hz and analyzed (PowerLab 2/25; AD instruments, New South Wales, Australia). Two steps of stimulus intensities (ISCEV standard; scotopic 0.01 and scotopic 3.0) were used for evaluating rod and mixed cone and rod responses. The b-wave amplitude of the rod response and the a-wave amplitude of the mixed cone and rod response were analyzed.

### SD-OCT

After ERG recording, rabbits were placed on a platform such that the visual streaks, which were approximately 3 mm ventral to the ONH, were located at the center of the image. The SD-OCT machine used in this study was *Multiline* OCT (Heidelberg Engineering, Heidelberg, Germany), which was customized based on a Spectralis HRA+OCT [37]. The *Multiline* OCT uses an 870-nm super-luminescent diode as a light source. The scan rate of the SD-OCT was 47,000 A-scans per second, with an axial resolution of ~7 μm.

### Measurement and evaluations of total retinal thickness by using SD-OCT

To measure the total retinal thickness at the visual streak, a volume scan image was obtained (Fig. S2A). The lines of the vitreoretinal interface and BM were manually delineated at each horizontal section in a masked fashion (Figs. S2B and S2C). The mean total retinal thickness was measured within a red circle 1 mm in diameter, the center of which was 3 mm ventral to the inferior edge of the ONH, as determined by the software supplied by Heidelberg Engineering (Figs. S2D and S2E).

### Measurements and evaluation of the thickness of retinal layers on vertical SD-OCT images

To measure and assess the thickness of each retinal layer, vertical OCT images, which passed through the center of the ONH and included the visual streak, were obtained by averaging 100 B-scans. To measure the thickness of the ONL, ELM–BM, INL, and GCC, the boundary lines between the OPL and ONL, ELM and BM, IPL and INL, and the vitreoretinal interface and IPL were manually delineated in a masked fashion (Fig. S3). The thickness of each retinal layer within the areas (0.5 mm each) 4 mm ventral to the lower edge of the ONH was measured as a function of distance from the lower optic disc margin by using the software supplied by Heidelberg Engineering (Fig. S3).

### Electron Microscopy

The enucleated rabbit eyes were fixed in the same manner as the H&E stain. The eyes were subsequently fixed in 1% osmium tetroxide for 90 min. The retina was dehydrated through a graded series of ethanol (50–100%), cleared in propylene oxide, and embedded in epoxy resin. Ultrathin sections were cut by using an ultramicrotome and stained with uranyl acetate and lead citrate. For ultrastructural immunohistochemistry, the enucleated RP rabbit eyes were fixed in 4% paraformaldehyde and 0.05% glutaraldehyde for 4 h. The fixed retina was cut with a microslicer (Microslicer DTK-1000, Dosaka EM, Kyoto, Japan) into sections with a thickness of 65 μm. The sections were incubated with mouse monoclonal anti-rhodopsin antibody (Ret-P1 (sc-57433), Santa Cruz, California, U.S.A.) and subsequently, with gold-conjugated Fab fragment of goat anti-mouse IgG (Nanogold, Molecular Probes, Inc., Oregon, U.S.A.), followed by silver enhancement (HQ Silver, Nanoprobes, Inc., New York, U.S.A.). The stained sections were observed by transmission electron microscopy (H-7650, Hitachi Co., Tokyo, Japan).

### Statistical analysis

Data from WT and RP rabbits were analyzed with an unpaired *t*-test by using PASW Statistics version 18.0 (SPSS Inc., Chicago, IL). The level of statistical significance was set at $P<0.05$.

## Supporting Information

**Figure S1 Ultrastructure of photoreceptors in 20-week-old WT and RP rabbits.** (A, B) Ultrastructure of photoreceptors in 20-week-old WT rabbits. The inner segments of photoreceptors (IS) and the outer segments of photoreceptors (OS) were regular and dense. (C, D) Ultrastructural changes in 20-week-old RP rabbits. The IS and OS were mostly absent, and the residual IS and OS were less organized than those in WT rabbits. In the magnified image (D), many small vesicles (arrowheads) appeared to be cleaved from the IS into the extracellular space around the photoreceptors (arrows).
(TIF)

**Figure S2 Measurement of mean total retinal thickness.** (A) An infrared image on volume scan mode of SD-OCT. In the volume scan mode, the region ventral to the optic disc, including visual streak (19 lines in vertical 15°× horizontal 30°) was imaged. (B) One of the 19 horizontal OCT sections on volume scan mode. The lines of the vitreoretinal interface and the Bruch's membrane are manually delineated at each horizontal section (C). (D) The retinal thickness map constructed from the volume scan OCT images. Total retinal thickness was measured within the red circle shown (E). The diameter of the red circle was 1 mm, and the center was 3 mm ventral to the inferior edge of the ONH (D, E).
(TIF)

**Figure S3 Measurement of the thickness of individual retinal layers.** Four vertical OCT sections that pass through the center of the ONH and visual streak are shown. On each section, the boundary lines between each retinal layer were manually delineated. The ONL, ELM–BM, INL, and GCC thicknesses were evaluated in 0.5-mm segments as a function of the distance from the inferior optic disc margin up to 4.0 mm ventral to the inferior edge of the ONH. ONL, outer nuclear layer; ELM, external limiting membrane; BM, Bruch's membrane; INL, inner nuclear layer; and GCC, ganglion cell complex.
(TIF)

## Acknowledgments

We thank MichikoTsuji, Yuri Terado, and Noriko Suzuki for their technical assistance; Megan Oliver for critical reading of the manuscript; Yuji Nishizawa of Chubu University for his advice on immunohistochemistry; and Gerhald Zinser of Heidelberg Engineering for discussion on the *Multiline* OCT. Presented in part at the Association Research in Vision and Ophthalmology (ARVO) Annual Meeting, May 2011; Florida, U.S.A.

## Author Contributions

Conceived and designed the experiments: HOI YM NY. Performed the experiments: YM NN MH MK HT AK. Analyzed the data: YM. Contributed reagents/materials/analysis tools: YT KOF HK. Wrote the paper: YM HOI.

## References

1. Hartong DT, Berson EL, Dryja TP (2006) Retinitis pigmentosa. Lancet 368: 1795–1809.
2. Mendes HF, van der Spuy J, Chapple JP, Cheetham ME (2005) Mechanisms of cell death in rhodopsin retinitis pigmentosa: implications for therapy. Trends Mol Med 11: 177–185.
3. Petters RM, Alexander CA, Wells KD, Collins EB, Sommer JR, et al. (1997) Genetically engineered large animal model for studying cone photoreceptor survival and degeneration in retinitis pigmentosa. Nat Biotechnol 15: 965–970.
4. Narfström K (1983) Hereditary progressive retinal atrophy in the Abyssinian cat. J Hered 74: 273–276.
5. Chader GJ (2002) Animal models in research on retinal degenerations: past progress and future hope. Vision Res 42: 393–399.
6. Petersen-Jones SM (1998) Animal models of human retinal dystrophies. Eye (Lond) 12(Pt 3b): 566–570.
7. Barnett KC, Curtis R (1985) Autosomal dominant progressive retinal atrophy in Abyssinian cats. J Hered 76: 168–170.
8. Menotti-Raymond M, David VA, Schäffer AA, Stephens R, Wells D, et al. (2007) Mutation in CEP290 discovered for cat model of human retinal degeneration. J Hered 98: 211–220.
9. Kijas JW, Cideciyan AV, Aleman TS, Pianta MJ, Pearce-Kelling SE, et al. (2002) Naturally occurring rhodopsin mutation in the dog causes retinal dysfunction and degeneration mimicking human dominant retinitis pigmentosa. Proc Natl Acad Sci U S A 99: 6328–6333.
10. Ng YF, Chan HH, Chu PH, To CH, Gilger BC, et al. (2008) Multifocal electroretinogram in rhodopsin P347L transgenic pigs. Invest Ophthalmol Vis Sci 49: 2208–2215.
11. Famiglietti EV, Sharpe SJ (1995) Regional topography of rod and immunocytochemically characterized "blue" and "green" cone photoreceptors in rabbit retina. Vis Neurosci 12: 1151–1175.
12. Rockhill RL, Daly FJ, MacNeil MA, Brown SP, Masland RH (2002) The diversity of ganglion cells in a mammalian retina. J Neurosci 22: 3831–3843.
13. Marc RE (1986) Neurochemical stratification in the inner plexiform layer of the vertebrate retina. Vision Res 26: 223–238.
14. Vaney DI, Young HM, Gynther IC (1991) The rod circuit in the rabbit retina. Vis Neurosci 7: 141–154.
15. Osakada F, Hirami Y, Takahashi M (2009) Stem cell biology and cell transplantation therapy in the retina. Biotechnol Genet Eng Rev 26: 297–334.
16. Stanzel BV, Liu Z, Brinken R, Braun N, Holz FG, et al. (2012) Subretinal delivery of ultrathin rigid-elastic cell carriers using a metallic shooter instrument and biodegradable hydrogel encapsulation. Invest Ophthalmol Vis Sci 53: 490–500.
17. Acland GM, Aguirre GD, Ray J, Zhang Q, Aleman TS, et al. (2001) Gene therapy restores vision in a canine model of childhood blindness. Nat Genet 28: 92–95.
18. Tao W, Wen R, Goddard MB, Sherman SD, O'Rourke PJ, et al. (2002) Encapsulated cell-based delivery of CNTF reduces photoreceptor degeneration in animal models of retinitis pigmentosa. Invest Ophthalmol Vis Sci 43: 3292–3298.
19. Bush RA, Lei B, Tao W, Raz D, Chan CC, et al. (2004) Encapsulated cell-based intraocular delivery of ciliary neurotrophic factor in normal rabbit: dose-dependent effects on ERG and retinal histology. Invest Ophthalmol Vis Sci 45: 2420–2430.
20. Kondo M, Sakai T, Komeima K, Kurimoto Y, Ueno S, et al. (2009) Generation of a transgenic rabbit model of retinal degeneration. Invest Ophthalmol Vis Sci 50: 1371–1377.
21. Wojtkowski M, Bajraszewski T, Gorczynska I, Targowski P, Kowalczyk A, et al. (2004) Ophthalmic imaging by spectral optical coherence tomography. Am J Ophthalmol 138: 412–419.
22. Chen TC, Cense B, Pierce MC, Nassif N, Park BH, et al. (2005) Spectral domain optical coherence tomography: ultra-high speed, ultra-high resolution ophthalmic imaging. Arch Ophthalmol 123: 1715–1720.
23. Sakamoto A, Hangai M, Yoshimura N (2008) Spectral-domain optical coherence tomography with multiple B-scan averaging for enhanced imaging of retinal diseases. Ophthalmology 115: 1071–1078.

24. Hangai M, Yamamoto M, Sakamoto A, Yoshimura N (2009) Ultrahigh-resolution versus speckle noise-reduction in spectral-domain optical coherence tomography. Opt Express 17: 4221–4235.
25. Byeon SH, Chu YK, Lee H, Lee SY, Kwon OW (2009) Foveal ganglion cell layer damage in ischemic diabetic maculopathy: correlation of optical coherence tomographic and anatomic changes. Ophthalmology 116: 1949–1959.
26. Nakano N, Hangai M, Nakanishi H, Mori S, Nukada M, et al. (2011) Macular Ganglion Cell Layer Imaging in Preperimetric Glaucoma with Speckle Noise-Reduced Spectral Domain Optical Coherence Tomography. Ophthalmology 118: 2414–2426.
27. Sandberg MA, Brockhurst RJ, Gaudio AR, Berson EL (2005) The association between visual acuity and central retinal thickness in retinitis pigmentosa. Invest Ophthalmol Vis Sci 46: 3349–3354.
28. Costa RA, Calucci D, Skaf M, Cardillo JA, Castro JC, et al. (2004) Optical coherence tomography 3: Automatic delineation of the outer neural retinal boundary and its influence on retinal thickness measurements. Invest Ophthalmol Vis Sci 45: 2399–2406.
29. Chen TC, Cense B, Miller JW, Rubin PA, Deschler DG, et al. (2006) Histologic correlation of in vivo optical coherence tomography images of the human retina. Am J Ophthalmol 141: 1165–1168.
30. Oishi A, Hata M, Shimozono M, Mandai M, Nishida A, et al. (2010) The significance of external limiting membrane status for visual acuity in age-related macular degeneration. Am J Ophthalmol 150: 27–32.
31. Murakami T, Nishijima K, Sakamoto A, Ota M, Horii T, et al. (2011) Association of pathomorphology, photoreceptor status, and retinal thickness with visual acuity in diabetic retinopathy. Am J Ophthalmol 151: 310–317.
32. Huber G, Beck SC, Grimm C, Sahaboglu-Tekgoz A, Paquet-Durand F, et al. (2009) Spectral domain optical coherence tomography in mouse models of retinal degeneration. Invest Ophthalmol Vis Sci 50: 5888–5895.
33. Kim KH, Puoris'haag M, Maguluri GN, Umino Y, Cusato K, et al. (2008) Monitoring mouse retinal degeneration with high-resolution spectral-domain optical coherence tomography. J Vis 8: 17 1–11.
34. Ruggeri M, Wehbe H, Jiao S, Gregori G, Jockovich ME, et al. (2007) In vivo three-dimensional high-resolution imaging of rodent retina with spectral-domain optical coherence tomography. Invest Ophthalmol Vis Sci 48: 1808–1814.
35. Srinivasan VJ, Ko TH, Wojtkowski M, Carvalho M, Clermont A, et al. (2006) Noninvasive volumetric imaging and morphometry of the rodent retina with high-speed, ultrahigh-resolution optical coherence tomography. Invest Ophthalmol Vis Sci 47: 5522–5528.
36. Fischer MD, Huber G, Beck SC, Tanimoto N, Muehlfriedel R, et al. (2009) Noninvasive, in vivo assessment of mouse retinal structure using optical coherence tomography. PLoS ONE 4: 1–7.
37. Nakano N, Ikeda HO, Hangai M, Muraoka Y, Toda Y, et al. (2011) Longitudinal and Simultaneous Imaging of Retinal Ganglion Cells and Inner Retinal Layers in a Mouse Model of Glaucoma Induced by N-Methyl-D-Aspartate. Invest Ophthalmol Vis Sci 52: 8754–8762.
38. Yamauchi Y, Agawa T, Tsukahara R, Kimura K, Yamakawa N, et al. (2011) Correlation between high-resolution optical coherence tomography (OCT) images and histopathology in an iodoacetic acid-induced model of retinal degeneration in rabbits. Br J Ophthalmol 95: 1161–1165.
39. Li T, Snyder WK, Olsson JE, Dryja TP (1996) Transgenic mice carrying the dominant rhodopsin mutation P347S: evidence for defective vectorial transport of rhodopsin to the outer segments. Proc Natl Acad Sci U S A 93: 14176–14181.
40. Aleman TS, Cideciyan AV, Sumaroka A, Windsor EA, Herrera W, et al. (2008) Retinal laminar architecture in human retinitis pigmentosa caused by Rhodopsin gene mutations. Invest Ophthalmol Vis Sci 49: 1580–1590.
41. Milam AH, Li ZY, Fariss RN (1998) Histopathology of the human retina in retinitis pigmentosa. Prog Retin Eye Res 17: 175–205.
42. Humayun MS, Prince M, de Juan E, Jr., Barron Y, Moskowitz M, et al. (1999) Morphometric analysis of the extramacular retina from postmortem eyes with retinitis pigmentosa. Invest Ophthalmol Vis Sci 40: 143–148.

# Transcorneal Electrical Stimulation Promotes Survival of Photoreceptors and Improves Retinal Function in Rhodopsin P347L Transgenic Rabbits

*Takeshi Morimoto,[1] Hiroyuki Kanda,[1] Mineo Kondo,[2] Hiroko Terasaki,[3] Kohji Nishida,[4] and Takashi Fujikado[1]*

**Purpose.** To determine whether transcorneal electrical stimulation (TES) has neuroprotective effects on the photoreceptors, and whether it slows the rate of decrease of the electroretinogram (ERG) in rhodopsin P347L transgenic (Tg) rabbits.

**Methods.** Six-week-old Tg rabbits received TES through a contact lens electrode on the left eye weekly for 6 weeks. The right eyes received sham stimulation on the same days. Electroretinograms (ERGs) were recorded before and at 12 weeks after the TES. After the last ERG recordings, the animals were euthanized for morphologic analysis of the retinas. Immunohistochemical (IHC) analysis was performed to detect the immunostaining by peanut agglutinin (PNA) and rhodopsin antibodies in the retinas.

**Results.** The a- and b-wave amplitudes of the photopic ERGs and the b-wave amplitudes of the scotopic ERGs at higher stimulus intensities were significantly larger in the TES eyes than in the sham stimulated eyes ($P < 0.05$, respectively). Morphologic analyses showed that the mean thickness of the outer nuclear layer (ONL) in the visual streak at 12 weeks was significantly thicker in TES eyes than in sham-stimulated eyes ($P < 0.05$). IHC showed that the immunostaining by PNA and rhodopsin antibody in the TES-treated retinas was stronger than that in the sham-stimulated retinas.

**Conclusions.** TES promotes the survival of photoreceptors and preserves the ERGs in Tg rabbits. Although further investigations are necessary before using TES on patients, these findings indicate that TES should be considered for therapeutic treatment for RP patients with a P347L mutation of rhodopsin. (*Invest Ophthalmol Vis Sci.* 2012;53:4254–4261) DOI: 10.1167/iovs.11-9067

Patients with RP have a progressive loss of rod and cone photoreceptors that leads to a severe decrease in the visual acuity and a severe constriction of the visual field.[1,2] The worldwide prevalence of RP is approximately 1 in 4000, meaning that more than 1 million individuals are affected worldwide.[3] As such, RP is one of the leading causes of blindness in the world.

Many promising treatments to save or restore vision in RP patients are being investigated clinically and experimentally.[4–9] Electrical stimulation (ES) of the retina is one of the methods that is being tried because it is less invasive than other treatments and has been shown to have neuroprotective properties on the visual system.[10–18] ES of the transected optic nerve stump in rats promoted the survival of axotomized retinal ganglion cells (RGCs) in vivo.[10] Transcorneal electrical stimulation (TES) in rats was reported to rescue axotomized RGCs[11,12] and promote axonal regeneration of injured RGCs.[13,14] TES was also shown to improve the visual function of patients with traumatic optic neuropathy and nonarteritic ischemic optic neuropathy.[15]

We have demonstrated that TES promoted the survival of photoreceptors and preserved the retinal function of Royal College of Surgeons (RCS) rats, an animal model of RP.[16] Ni et al.[17] also reported that TES had neuroprotective effects on the photoreceptors after phototoxicity in rats. In a preliminary clinical trial, Schatz et al.[18] demonstrated that TES improved the visual function in RP patients.

However, RP is a genetically heterogeneous disease, and mutations in several photoreceptor-specific and some non-specific genes are known to cause RP.[19] Therefore, it is necessary to examine the neuroprotective effect of TES on the photoreceptors in the retinas of various RP animal models to determine which genetic type of RP is responsive to TES.

Rhodopsin Pro 347 Leu (P347L) transgenic (Tg) rabbits have been generated by Kondo et al.[20] This sequence of alterations is similar to those in human patients with autosomal dominant RP (adRP) with the rhodopsin P347L mutation.[21,22] This animal model has a rod-dominated, progressive photoreceptor degeneration with regional variations in the pattern of photoreceptor loss.[20,23]

The purpose of this study was to determine whether TES has a neuroprotective effect on the photoreceptors and improves the amplitudes of the electroretinogram (ERG) in Tg rabbits. Our morphologic and electrophysiological analyses showed that TES had a neuroprotective effect on the photoreceptors and improved the amplitudes of the ERG of Tg rabbits.

## Materials and Methods

### Animals

All experimental procedures were performed in accordance with the ARVO Statement for the Use of Animals in Ophthalmic and Vision

From the [1]Departments of Applied Visual Science and [4]Ophthalmology, Osaka University Graduate School of Medicine, Osaka, Japan; [2]Department of Ophthalmology, Mie University Graduate School of Medicine, Mie, Japan; and [3]Department of Ophthalmology, Nagoya University Graduate School of Medicine, Nagoya, Japan.

Submitted for publication November 12, 2011; revised April 3, 2012; accepted April 25, 2012.

Disclosure: **T. Morimoto**, None; **H. Kanda**, None; **M. Kondo**, None; **H. Terasaki**, None; **K. Nishida**, None; **T. Fujikado**, None

Corresponding author: Takeshi Morimoto, Department of Applied Visual Science, Osaka University Graduate School of Medicine, 2-2 Yamadaoka, Suita City, Osaka 565-0871, Japan; takeshi.morimoto@ophthal.med.osaka-u.ac.jp.

Research, and the procedures were approved by the Animal Research Committee, Osaka University Graduate School of Medicine. Five Tg rabbits were purchased from the Kitayama Labes Co. (Ina, Japan). They were raised on a 12-hour dark 12-hour light cycle with an ambient light intensity of 100 lux.

### Transcorneal Electrical Stimulation

The rabbits were anesthetized intramuscularly with a mixture of medetomidine (0.3 mg/kg, Domitor; Orion Corporation, Espoo, Finland), midazolam (4 mg/kg, Dormicum, Astellas Pharma Inc., Tokyo, Japan), and butorphanol (5 mg/kg, Betorphal; Meiji Seika Pharma, Co., Ltd., Tokyo, Japan). For the electrical stimulation, the corneas were also anesthetized with a drop of 0.4% oxybuprocaine HCl, and a contact lens electrode with inner and outer concentric electrodes (Mayo Corporation, Nagoya, Japan) was placed on the cornea with a drop of 2.5% methylcellulose to maintain good electrical contact and prevent corneal drying. Biphasic rectangular current pulses (700 μA, 10 ms/phase duration) were delivered at a frequency of 20 Hz from an electrical stimulation system (Stimulator: SEN-7320, Nihon Kohden, Tokyo, Japan; Isolator: WPI, Sarasota, FL) through the contact lens electrode.

TES was given to 6-week-old rabbits for 1 hour once a week until the animals were 12 weeks old. Only the left eye was electrically stimulated. The same type of contact lens electrode was placed on the right eyes but no electrical current was delivered (sham stimulation).

### Electroretinograms

ERGs were recorded from the animals at 6 weeks of age just before the beginning of the TES and after the end of the TES treatments at 12 weeks of age. For the TES, animals were anesthetized intramuscularly with a mixture of medetomidine (0.3 mg/kg), midazolam (1 mg/kg), and butorphanol (1 mg/kg). The pupils were dilated with 2.5% phenylephrine hydrochloride and 0.5 % tropicamide.

After 1 hour of dark adaptation, the animals were restrained in a box and were prepared for the recordings under dim red light. ERGs were recorded from both eyes simultaneously with a corneal electrode carrying LEDs creating a mini-Ganzfeld stimulator (WLS-20, Mayo Corporation). A 2.5% hydroxypropyl methylcellulose ophthalmic solution was used with the corneal contact lens electrode. The reference electrode and a ground electrode were inserted subcutaneously into the left ear and the nose, respectively.

The luminance of the scotopic ERG stimuli was increased from −5.0 to 1.48 log cd·s/m$^2$ in 0.5 or 1.0 log unit steps. After the scotopic ERG recordings, animals were light-adapted for 30 minutes, and the photopic ERGs were recorded. The luminance of photopic ERG stimuli was increased from −1.0 to 1.95 log cd·s/m$^2$, and the stimuli were presented on a white background of 25 cd/m$^2$.

The responses were amplified, band pass filtered from 0.3 to 1000 Hz, and digitized at 3.3 kHz. A computational ERG recording system (Neuropack μ; Nihon Kohden, Tokyo, Japan) was used to average the ERG responses. Five to 20 responses were averaged with interstimulus intervals from 1 to 10 seconds depending on the intensity of the stimulus.

### ERG Analysis

The scotopic (dark-adapted) and photopic (light-adapted) a-wave amplitudes were measured from the prestimulus baseline to the peak of the a-wave, and the b-wave amplitude was measured from the trough of the a-wave to the peak of b-wave.

To determine the significance of differences in the ERG amplitudes between TES electrically stimulated eyes and sham-stimulated eyes for the full intensity range, we plotted the average ratio of the TES-treated to the sham-stimulated eyes at all intensities and performed statistical analyses.[22–24]

### Histological Analysis

Immediately after the final ERG recordings, the rabbits were euthanized with an overdose of pentobarbital sodium. The eyes were removed and placed in a mixture of 10% neutral buffered formalin and 2.5% glutaraldehyde in 0.1 M phosphate buffer (PB) for 30 minutes at room temperature. Then eyes were trimmed, and part of the eye cups, including the optic nerve, were postfixed in 4% glutaraldehyde in 0.1 M PB at 4°C. The tissues were trimmed, embedded in paraffin, sectioned vertically, and stained with hematoxylin and eosin for light microscopy. All sections were cut along the vertical meridian of the eye passing through the optic nerve. Five serial sections of each eye were analyzed for each experimental animal.

The degree of retinal degeneration was assessed by measuring the thickness of the outer nuclear layer (ONL), inner nuclear layer (INL), and ganglion cell layer (GCL). Photographs were taken of the superior and inferior hemispheres at 10 defined points with a camera attached to a light microscope (E800; Nikon, Tokyo, Japan). The first photograph was taken at approximately 2 mm from the center of the optic nerve head, and subsequent photographs were taken every 2 mm more peripherally. The thickness of ONL, INL, and GCL were measured on the photographs (Scion Image analyzer; Scion Corp., Frederick, MD). Each eye was coded so that the investigator making the measurements was masked to treatment of the eye.

### Immunohistochemistry

The paraffin-embedded sections (5 μm) were processed for immunofluorescence staining with antirhodopsin antibody (1:100; RETP1; Santa Cruz Biotechnology, Santa Cruz, CA), followed by Cy3-conjugated anti-mouse IgG (1:200), and FITC-conjugated peanut agglutinin (1:100) (PNA; Invitrogen, Carlsbad, CA), a lectin that binds specifically to rabbit cone photoreceptors. The TES-treated and sham-stimulated sections were observed with a fluorescence microscope (E800; Nikon).

### Statistical Analysis

Data were analyzed with a commercial software (JMP8; SAS Institute Japan, Tokyo, Japan). The data were expressed as the means ± SDs or SEMs. Comparisons between two groups were made by Student's *t*-tests when the data were normally distributed or by the Mann-Whitney rank-sum test when the data were not normally distributed. Statistical significance was set at $P < 0.05$.

## Results

### Effect of TES on Survival of Photoreceptors in Tg Rabbits

Representative retinal sections in the area of the visual streak from 12-week-old Tg rabbits that had TES (left eye) or sham stimulation (right eye) are shown in Figures 1A and 1B. The number of rows of nuclei in the ONL at the visual streak was two to three and the nuclei were closely packed in the retina receiving TES (Fig. 1A). In the sham-stimulated retina, only one row of nuclei was found in the ONL at the visual streak and they were loosely packed (Fig. 1B). In contrast, there was no difference in the structure and thickness of the ONL in other areas of the retina away from the visual streak between the TES-treated and sham-stimulated retinas (Figs. 1C, 1D). The architecture and thickness of the middle and inner retinal layers were well preserved in both TES-treated and sham-stimulated retinas (Figs. 1A–D).

Quantitative analyses showed that the thickness of the ONL in the visual streak in the TES-treated eyes was 13.9 ± 3.3 μm

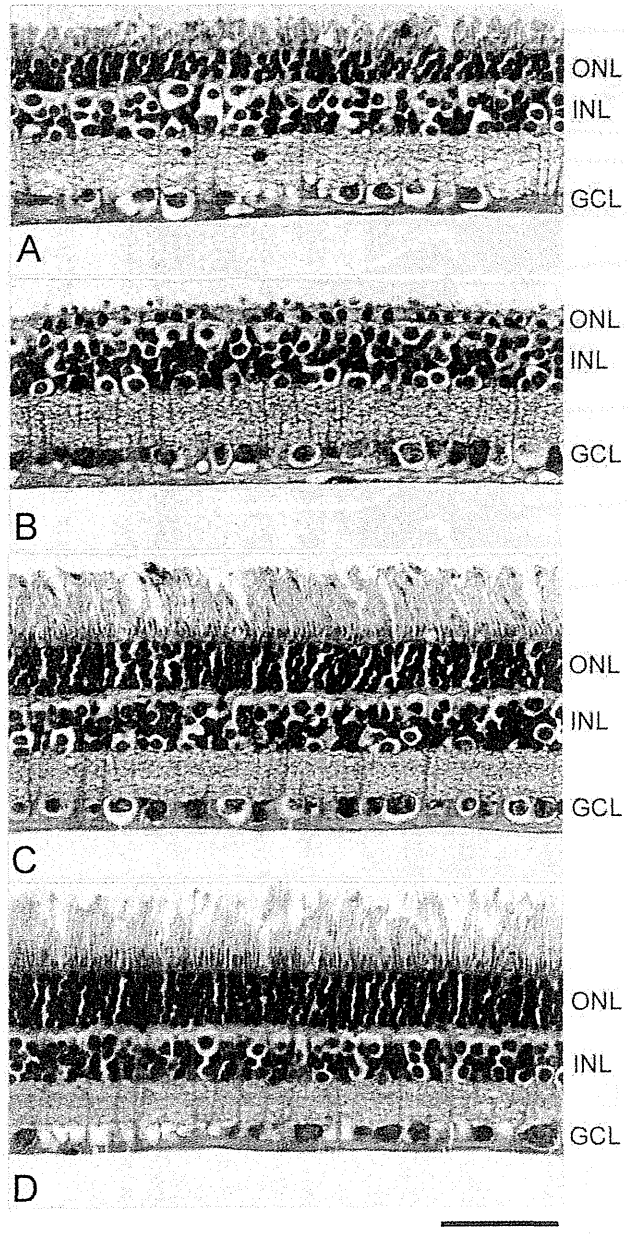


FIGURE 1. Photomicrographs of TES-treated and sham-stimulated retinas from 12-week-old Tg rabbits. Retinal sections of the visual streak from TES-treated retina (**A**) and sham-stimulated retina (**B**). Peripheral retinas at 6 mm superior to the optic nerve head from TES-treated retina (**C**) and sham-stimulated retina (**D**). Scale bar = 50 μm.

(mean ± SD, $n = 5$) which was significantly thicker than that in the sham-stimulated eyes (8.8 ± 2.8 μm, $n = 5$, $P < 0.05$) (inferior hemisphere 1). In contrast, there was no significant difference in the mean ONL thickness outside the area of the visual streak (Fig. 2A). Thus, TES promoted the survival of photoreceptors in the area of the visual streak at 12 weeks of age.

To determine whether TES affected other layers of the retina, we measured the thickness of the INL and GCL. There were no significant differences of the mean thickness of INL and GCL between the TES retinas and in the sham retinas ($n = 5$ each; Figs. 2B, 2C).

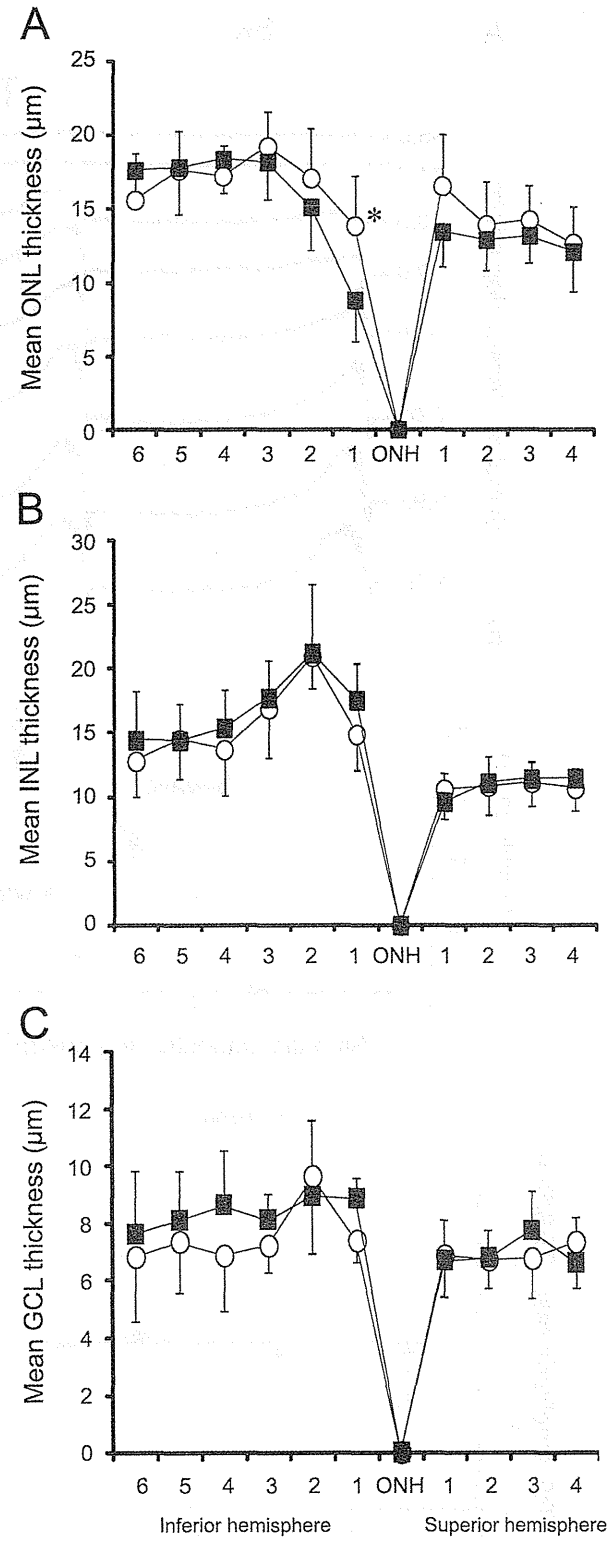


FIGURE 2. Thickness of the ONL (**A**), the INL (**B**), and the GCL (**C**) along the vertical meridian measured at 10 retinal locations at 2-mm intervals. Mean ± SD of five Tg rabbits are plotted. There was a significant difference of the mean ONL thickness between TES-treated retinas (○) and sham-stimulated retina (■) at the visual streak (Student's *t*-test for two groups; $^*P < 0.05$).